THE OPTICAL SPECTROSCOPIC AND PHOTOMETRIC OBSERVATIONS OF THE OPTICAL COUNTERPARTS TO THE BE/X-RAY BINARY SYSTEMS: GRO J2058+42 AND V0332+53

A THESIS SUBMITTED TO
THE GRADUATE SCHOOL OF NATURAL AND APPLIED SCIENCES
OF
MIDDLE EAST TECHNICAL UNIVERSITY

BY

MEHTAP ÖZBEY

IN PARTIAL FULFILLMENT OF THE REQUIREMENTS
FOR
THE DEGREE OF MASTER OF SCIENCE
IN
PHYSICS

AUGUST 2008

Approval of the thesis

THE OPTICAL SPECTROSCOPIC AND PHOTOMETRIC OBSERVATIONS OF THE OPTICAL COUNTERPARTS TO THE BE/X-RAY BINARY SYSTEMS: GRO J2058+42 AND V0332+53

Submitted by **MEHTAP ÖZBEY** in partial fulfillment of the requirements for the degree of **Master of Science in Physics Department, Middle East Technical University**, by

Prof. Dr. Canan Özgen
Dean, Graduate School of **Natural and Applied Sciences** _____

Prof. Dr. Sinan Bilikmen
Head of Department, **Physics** _____

Prof. Dr. Ümit Kızıloğlu
Supervisor, **Physics Dept., METU** _____

Examining Committee Members:

Prof. Dr. Ethem Derman
Astronomy and Space Sciences Dept., Ankara U. _____

Prof. Dr. Ümit Kızıloğlu
Physics Dept., METU _____

Prof. Dr. Halil Kırbıyık
Physics Dept., METU _____

Prof. Dr. Nilgün Kızıloğlu
Physics Dept., METU _____

Assist. Prof. Dr. Sıtkı Çağdaş İnam
Electrical and Electronics Engineering Dept., Başkent U. _____

Date: _____

I hereby declare that all information in this document has been obtained and presented in accordance with academic rules and ethical conduct. I also declare that, as required by these rules and conduct, I have fully cited and referenced all material and results that are not original to this work.

Name, Last Name : Mehtap Özbey
Signature :

ABSTRACT

THE OPTICAL SPECTROSCOPIC AND PHOTOMETRIC OBSERVATIONS OF THE OPTICAL COUNTERPARTS TO THE BE/X-RAY BINARY SYSTEMS: GRO J2058+42 AND V0332+53

ÖZBEY, MEHTAP

M.S., Department of Physics

Supervisor: Prof. Dr. Ümit Kızıloğlu

August 2008, 68 pages

The spectroscopic and photometric observations of the optical counterparts to the Be/X-ray binary systems GRO J2058+42 and V0332+53 (BQ Cam), taken with RTT150 (Russian-Turkish 1.5 meter Telescope), are presented in this study. The distance, color and the reddening estimates for both sources, obtained via photometric observations, are consistent with the previous results. The results of our spectroscopic observations performed between May 2006 and June 2008 for optical counterpart to GRO J2058+42 indicate that the double-peaked emission line profile turns into a single-peaked emission after the last outburst of the system. Furthermore, the spectra of the source show clear evidence for the changes in the ratio of the double peaks of H_α emission line indicative of the precession of the high-density regions confined in the disk. Unlike the spectra of counterpart to GRO J2058+42, the spectra of BQ Cam, taken between September 2006 and December 2007, exhibit single-peaked H_α and HeI (λ7065 Å)emission lines. In addition, the equivalent width values of H_α emission lines, shifts from the the laboratory wavelengths for H_α and HeI

emission lines and the variation in optical brightness of BQ Cam show a close correlation.

Keywords: Be/X-ray Binaries, Be Stars, Emission Line-Stars, H_α Emission Line, Spectrum Analysis, V/R Variability, BQ Cam , GRO J2058+42

ÖZ

GRO J2058+42 VE V0332+53 BE/X-IŞIN ÇİFT SİSTEMLERİNİN OPTİK BİLEŞENLERİNİN TAYFSAL VE FOTOMETRİK GÖZLEMLERİ

ÖZBEY, MEHTAP

Yüksek Lisans, Fizik Bölümü

Tez Yöneticisi: Prof. Dr. Ümit Kızıloğlu

Ağustos 2008, 68 sayfa

Bu çalışmada GRO J2058+42 ve VO332+53 Be/X-ışın sistemlerinin optik bileşenlerinin, 1.5 metrelik Rus-Türk teleskopu ile yapılmış tayfsal ve fotometrik gözlemleri sunulmaktadır. Fotometrik gözlemlerle her iki kaynak için elde edilen uzaklık, renk ve kızarma değerleri daha önce belirtilmiş değerlerle uyumludur. GRO J2058+42 sisteminin optik bileşeninin Mayıs 2006-Haziran 2008 arasında yapılan gözlemlerinin tayfsal sonuçları H_α salma çizgisinin çift tepeli durumdan tek tepeli duruma geçtiğini göstermiştir. Ayrıca kaynağın tayflarında, diskte yeralan yüksek yoğunluklu bölgelerin devinimini kanıtlayan V/R değişimleri bulunmaktadır. GRO J2058+42 sistemindeki optik bileşenin aksine, BQ Cam'a ait Eylül 2006-Aralık 2007 tarihlerinde alınmış tayflarda ise, hem H_α hem de HeI çizgisi, tek tepeli salma olarak görülmektedir. Ayrıca H_α salma çizgisinin eşdeğer genişlik değerlerinin, H_α ve HeI salma çizgisinin laboratuar dalga boyundan olan kayma miktarı ve BQ Cam'in parlaklık değişimiyle korelasyon içinde bulunduğu görülmüştür.

Anahtar Kelimeler: Be/X-ışın Çiftleri, Be Yıldızları, Salma Çizgili Yıldızlar, H_α

To my family

ACKNOWLEDGMENTS

I would like to express my deep and sincere gratitude to my supervisor Prof. Dr. Ümit KIZILOĞLU for giving me a great chance and opportunity to work with him. Without his guidance and encouragement it would be harder to conclude this study. I would like to thank Assist. Prof. Dr. Sinan Kaan YERLİ and Prof. Dr. Nilgün KIZILOĞLU for their critical comments and advices about my thesis.

I am very grateful to my family for encouraging and supporting me all these years. I also would like to thank my uncle Hatip MOLAY who has never given up encouraging me since my childhood and also thank him for showing me the way of looking to life at different views.

I thank my colleagues and friends in METU Astrophysics Group for their support and friendship. I am grateful Kıvılcım Başak VURAL who became an special friend of mine. I also would like to thank Şeyda Şahiner for her support and friendship.

I especially thank Cemal ARABACI for his love, patience and understanding.

I acknowledge support from TÜBİTAK, The Scientific and Technological Research Council of Turkey, through project 106T040.

TABLE OF CONTENTS

LIST OF TABLES

TABLES

LIST OF FIGURES

FIGURES

CHAPTER 1

INTRODUCTION

As a class of X-ray binaries, HMXBs (High Mass X-ray Binaries) consist of a massive early type star (8 $M_{\odot}$ - 20 $M_{\odot}$) and an X-ray producing compact object such as a black hole or a NS (neutron star) which orbits around its companion. According to the evolutionary status of the optical companion there are two known types: 1)SHMXBs (Supergiant High Mass X-ray Binaries), where the massive star has filled its Roche-lobe and throws material towards the NS; 2)Be/X-ray Binaries, having a Be-star companion which is not substantially evolved has not filled its Roche-lobe in contrast to SHMXBs.

The analysis of the spectroscopic and photometric observations of two selected Be/X-ray binaries and spectroscopic observations of two selected spectrophotometric standard stars for comparison represented in this study were performed with RTT150[1].

General characteristics of Be/X-ray transient systems and disk models proposed so far are explained in this chapter. Historical background of the observed systems in this work and observational details are presented in Chapter 2 and Chapter 3. Chapter 4 includes the observational results with the comparison of two standard stars whereas conclusion of this study takes part in Chapter 5.

[1]RTT150: Russian-Turkish 1.5 meter Telescope

1.1 Be/X-ray Binaries

Be/X-ray binaries, outnumber systems in HMXBs, are the transient X-ray sources with a Be type star and a NS. Emission lines and strong infrared excess which indicate the existence of "decretion" disk around Be star are the main observational characteristics of these systems. Figure 1.1 represents a model of a typical Be/X-ray binary system.

The X-ray radiation in Be/X-ray systems is usually a pulsar operated by the material carried with stellar winds from the Be companion. Be/X-ray binaries show mainly three different types of X-ray activities (Stella et al. 1986):

i) Type I (Normal) outbursts:

Almost all Be/X-ray binaries produce Type I outbursts however in different forms (Okazaki & Negueruela 2001). Type I outbursts, characterized by lower X-ray luminosities ($L_x \approx 10^{36}$ - 10^{37} erg s^{-1}) generally occur near to the periastron passage of the neutron star and last from days to a week. Although Type I outbursts are displayed at every periastron passage of some systems with the durations equal to the orbital periods or their multiples , roughly less than 1%

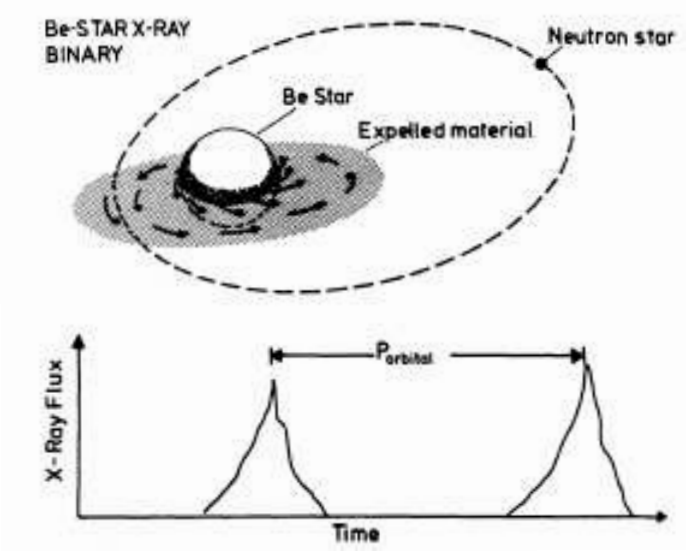

Figure 1.1: Schematic model of a Be/X-ray transient system (Slettebak 1988, adapted from van den Heuvel & Rappaport 1987).

of periastron passages results in Type I outbursts. On the other hand, short series of normal outbursts separated with long periods are the characteristic of some others (Ziólkowski 2002).

ii) Type II (Giant) outbursts:

They are known to have high X-ray luminosities ($L_x \gtrsim 10^{37}$ erg s^{-1}). Giant outbursts that do not exhibit individual orbital modulation (Finger & Prince 1997) last several weeks. Type II outbursts generally occur after an enhancement of magnitude of the optical companion. Although giant outbursts are attributed to the activity of Be star for this reason, in some systems the duration of giant outbursts correlated with their peak intensities (Negueruela 2004, Finger et al. 1996, Motch et al. 1991).

iii) Persistent low-luminosities:

Some systems that always seen in this state are permanent X-ray sources ($L_x \lesssim 10^{36}$ erg s^{-1}) have likely wide orbits ($P_{orb} \gtrsim 200$ days) and relatively long spin periods ($P_{spin} > 200$ s) (Raguzova & Lipunov 1998). However the systems having a fast spinning NS also show this type of weak X-ray luminosity.

The mass flux of the material thrown towards the NS is the determinative parameter that operates the type of X-ray activities mentioned above. The magnetosphere of the NS grows larger when the flux of falling material on the NS decreases. Since the dynamical pressure of the falling material is larger than the magnetic pressure of the NS, its clear that the NS should have much smaller magnetosphere at periastron passage than at apastron passage. In contrast to the apastron passage, at the periastron passage of the NS the equilibrium period (P_{eq}), defined as the period for which the corotation velocity at the magnetospheric radius equals to the Keplerian velocity, is smaller than the spin period of the NS ($P_{spin} > P_{eq}$; slow pulsar). As there is no centrifugal block, the falling material can come close to the NS and an accretion can take place around compact object. However at apastron passage, equilibrium period is bigger than the spin period of the NS ($P_{spin} < P_{eq}$; fast pulsar). In other words the falling materials which try to accrete will be forced to drive away from the NS by the

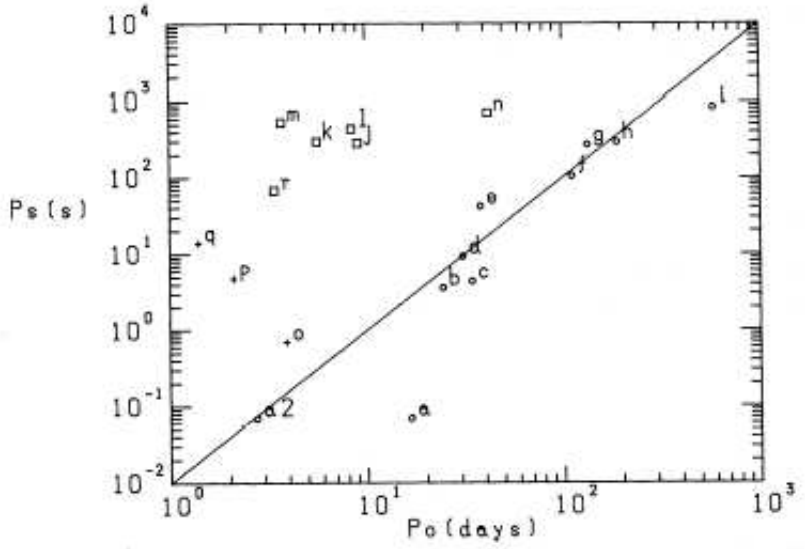

Figure 1.2: P_{orb}/P_{spin} diagram (Corbet 1986). The straight line indicates an empirical approximation to the relationship between P_{orb} and P_{spin}).

magnetospheric propeller. These mechanisms controlling the accretion rate of the material provided from the optical companion usually responsible for the Type I outbursts that repeat moderately with regular durations at or near the periastron passages. On the other hand Type II outbursts are related to the variation of decretion disk with time. The amount of outflowing material from the optical companion could increase in some occasions causing the instability of the disk and it leads to trigger the giant outbursts (Finger et al. 1996) during which the accretion disk is present.

In addition to these transient X-ray natures, some systems show persistent X-ray luminosity in their quiescent phase as well. The main reason of this weak luminosity, together with uncertainty, is thought to be the leakage of the material through the centrifugal barrier which generally occurs in the case of the fast spinning NSs (Campana et al. 2002).

The strong correlation between P_{orb} and P_{spin}, pointed out first by Corbet in 1984, is another characteristic for most of Be/X-ray binaries. It is seen from Figure 1.2 that Be/X-ray binaries fall within a narrow area in the P_{orb}/P_{spin} diagram known as "Corbet diagram" (Corbet 1986). The updated version of Cor-

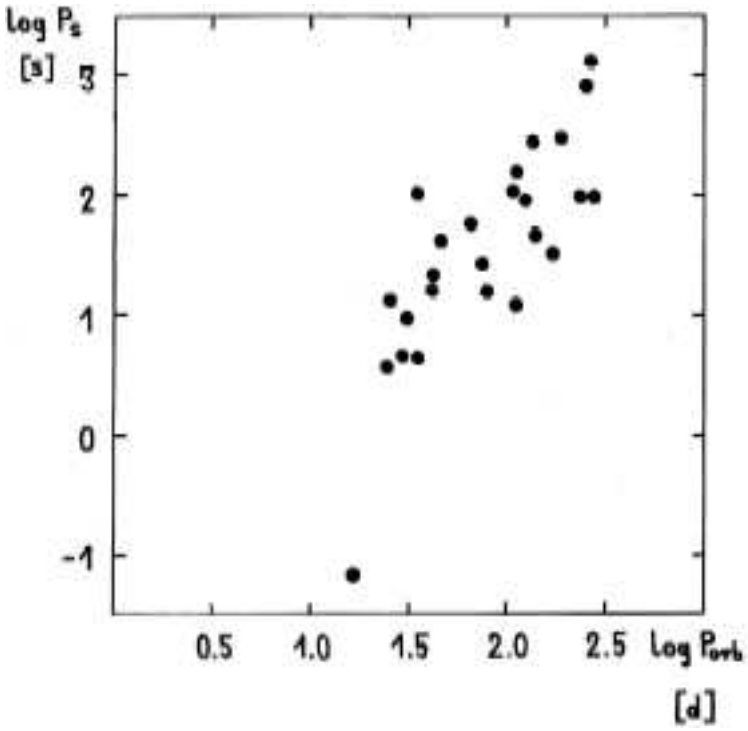

Figure 1.3: Corbet diagram updated by Ziólkowski 2002. The diagram contains 25 Be/X-ray systems of which both periods are presently known.

bet diagram (containing 25 Be/X-ray systems) published by Ziólkowski (2002) is shown in Figure 1.3. This correlation is an evidence for the fact that the NSs in Be/X-ray binaries rotate at the equilibrium velocity. As P_{eq} is inversely proportional to accretion rate ($P_{eq} \propto \dot{M}^{-3/7}$) the NS tries to adjust its spin period to the equilibrium period owing to the variation of the matter provided by its optical companion.

The latest catalogue of Be/X-ray systems and candidates was presented by Popov & Raguzova (2004). Figure 1.4 shows the observational results of that catalogue which contains 90 Be/X-ray systems (and candidates) over their orbital characteristics. The lack of systems with periods 10-20 days attributed to the effect of tidal synchronization in binaries (Raguzova & Lipunov 1998). The systems which have eccentricities in the range 0.4-0.5 are the most numerous ones among them.

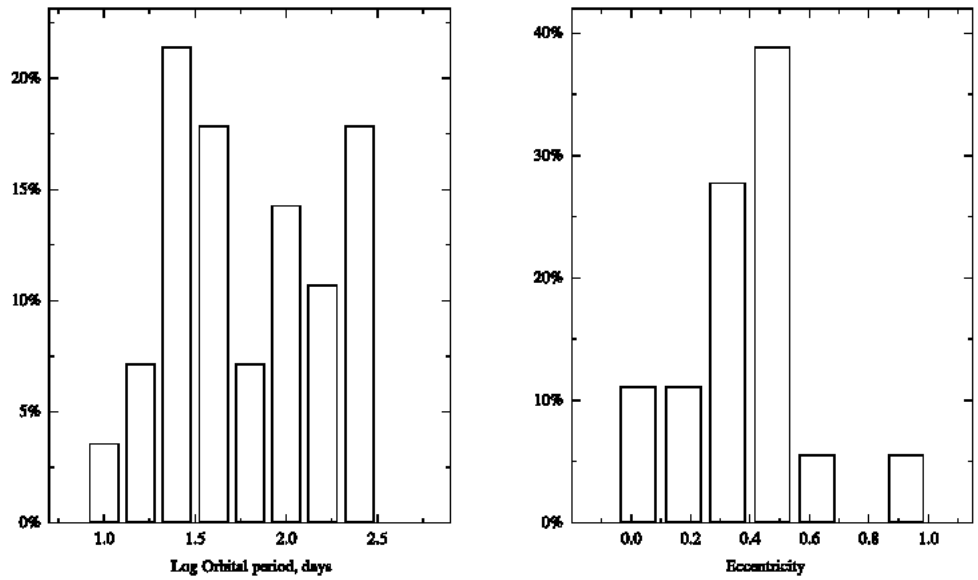

Figure 1.4: The distributions of number of observational Be/X-ray binaries over orbital periods (left) and eccentricities (right) take part in Be/X-ray catalogue (Popov & Raguzova 2004).

1.2 Be Stars in Binary Systems

A Be star is a non-supergiant early type star which shows or has shown (at a time in the past) Balmer lines in emission (typically double peaked) in its spectrum (Jaschek & Egret 1982, Collins 1987, Slettebak 1988, Porter & Rivinius 2003). In addition to Balmer lines, some singly ionized metallic lines such as FeII, SiII, MgII, and neutral helium lines might be seen in emission opposed to normal stars of the same spectral type. Indeed nowadays, Be term has been used for not only "B type stars having emission lines", but also "the stars that exist in luminosity classes III-V which are earlier than B type" (e.g. Oe type stars). In other words, "Be" definition refers to the general characteristics of a star that presents emission lines in its spectrum and some special features. The exact spectral and luminosity classification of a Be star is rather difficult due to the fact that rapid rotation broadens the lines in the spectrum (Slettebak 1978). Its known that Be type stars rotate at 70-80% of their critical velocities which correspond to roughly 400 km s^{-1} at their equator regions. Additionally, the

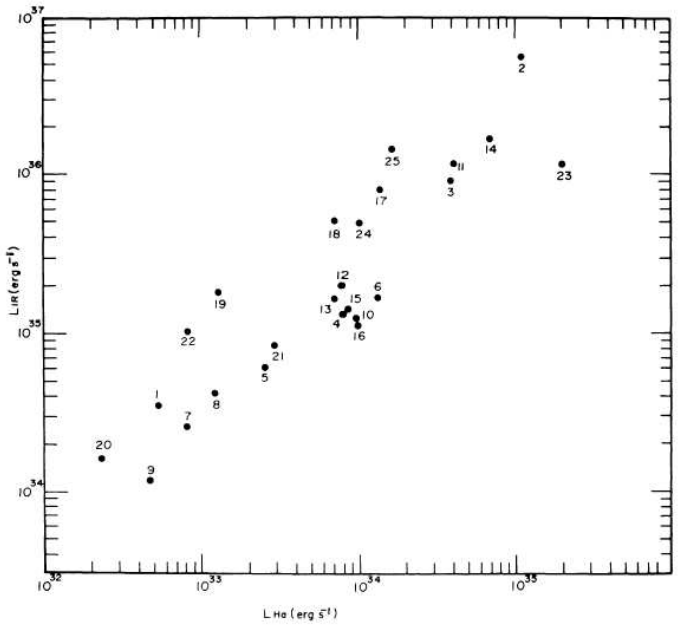

Figure 1.5: The correlation between IR luminosity (L_{IR}) and H_α luminosity (L_{H_α}) of some Be stars (Goraya & Rautela 1985).

gravity darkening and the oblateness which affect the evolutionary status of Be stars make them to appear more evolved due to this high rotation. Although the main reason of the high rotation has not been understood clearly, the new aspects about this subject were been obtained by Maeder (1999) and Heger Langer (2000). They emphasized that the outer layers of massive stars could spin up during their life on the main sequence due to the angular momentum evolution.

Photometric observations of Be type stars prove that they emit strong excess in the infrared (IR) region. While recombination of ionized Hydrogen is responsible for the emission lines in the spectrum, IR excess is due to free-free and bound-free radiation of recombination of ionised hydrogen (Scargle et al. 1978). Goraya & Rautela established the correlation between excess IR radiation and H_α emission using the observations of 25 selected sample of bright Be stars, in 1985 (Figure 1.5). This correlation which refers to the existence

of circumstellar disk around Be star is responsible for producing both emission lines and IR excess.

1.3 Disk Models

It is obvious that existence of decretion disk is the primary cause of unique properties (emission lines and IR excess) seen in the case of Be stars. The recent studies make several subjects clear about this phenomenon with the help of the technological developments on observational techniques. However the questions of why Be stars have a decretion disk and type of which mechanisms operate the disk structure have not yet been exactly answered. Even though any of them can be the answer of the questions individually, the different mechanisms and related models proposed so far to be the probable explanations are as follows;

1.3.1 Fast Rotation with Non-Radial Pulsation (Rotational Model & Non-Radial Pulsation Model)

Starting point of initial models are usually based on the rapid rotation of Be stars since it is an unexpected characteristic behavior. Struve's rotational model (Struve 1930 & 1931) was the first model to explain the relation between the emission lines and the disk). The spectroscopic observations verify the relation that the inclination angle of axis is responsible for seen emission lines with different shapes and widths in Be star's spectrum. With the increasing inclination angle, the shape of the emission lines is changing as single-peaked profile to double-peaked (Figure 1.6. The typical shell profile, characterized by "deep absorption cores embedded into certain emission lines (Hanuschik 1996)", seen in the bottom panel of the figure. For the material in the disk moves at right angles to the line of sight (viewing as equatorial-on), we observe narrow absorbtion lines in the spectrum. The projected rotational velocity ($V \sin(i)$) can be

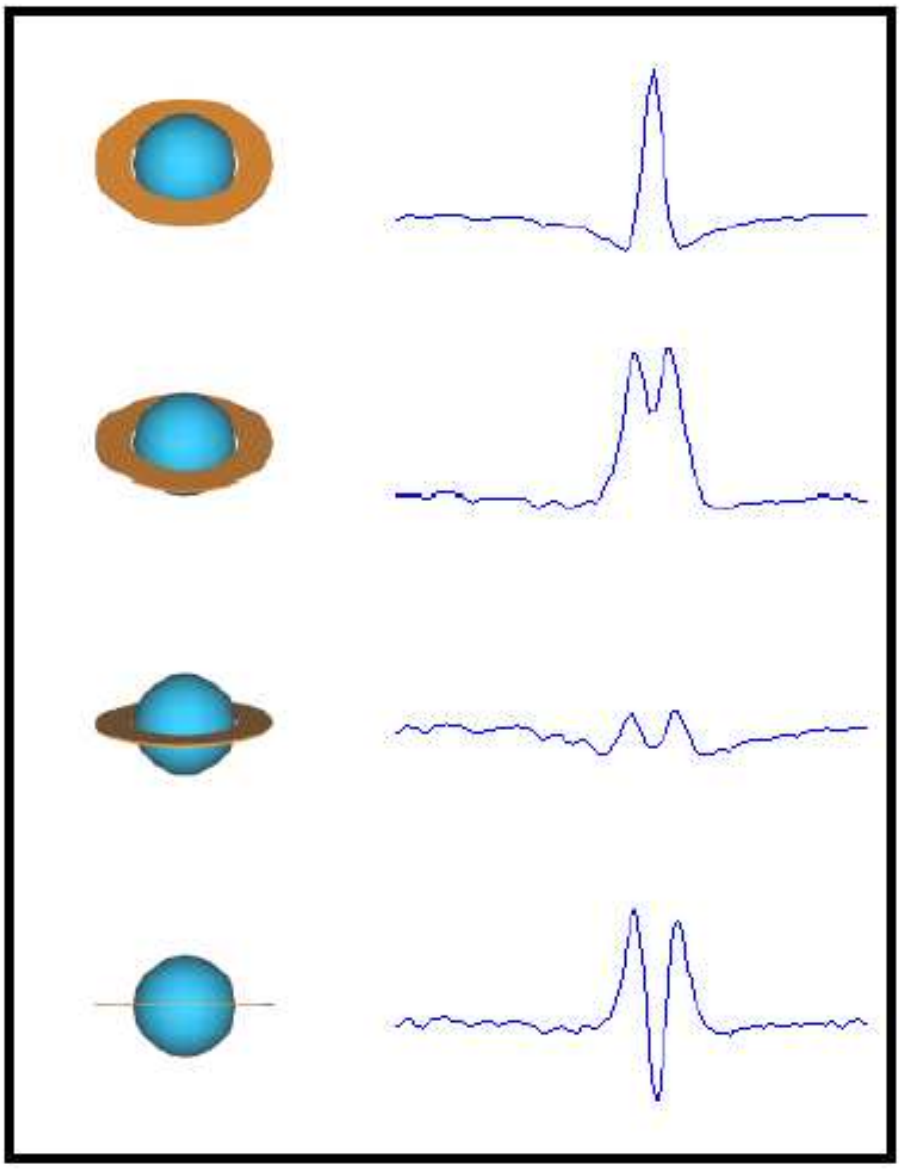

Figure 1.6: Struve's rotational model of a Be star (Struve 1930&1931). The rapidly-rotating Be star with equatorial gaseous shell(left) produces different emission line profiles (right), in function of the polar inclination from top to bottom (This figure is taken from http://www.astrosurf.com/buil/us/bestar.htm).

obtained by Buscombe's approximation (1969)

$$\frac{V\sin(i)}{c} = \frac{FWHM}{2\lambda_0(ln2)^{1/2}} \tag{1.1}$$

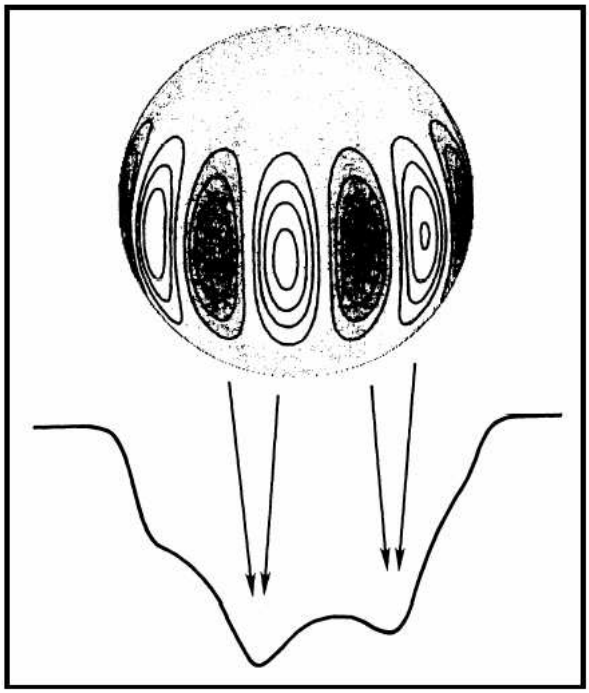

Figure 1.7: Illustration of the formation of distortions in the line profiles of a rapidly-rotating nonradially-oscillating star (Vogt & Penrod 1983). This figure is adopted from Slettebak 1988.

where λ_0 is the laboratory wavelength of the spectral line, $FWHM$ relates to the full width at half maximum and c is the speed of light.

Although centrifugal force of the star produces further outward pressure due to high rotation, this pressure is not sufficient to eject the material from the equatorial region of the Be star. Therefore non-radial pulsation is thought to be the required additional force to rotation to eject the materials. Also the observed short-term variabilities are attributed to non-radial pulsation of Be stars (Baade 1982, Baade et al. 2002, Rivinius et al. 2003). Recent works reveal that Be stars which show line profile variabilities are $l = m = 2$ mode pulsators. The effect of non-radial pulsation seen clearly in Figure 1.7 as the distortions in the line profile. While the darkest shaded regions correspond to material moving away from the observer, the lightest shaded regions shows material moving toward the observer (Vogt & Penrod 1983, Slettebak 1988).

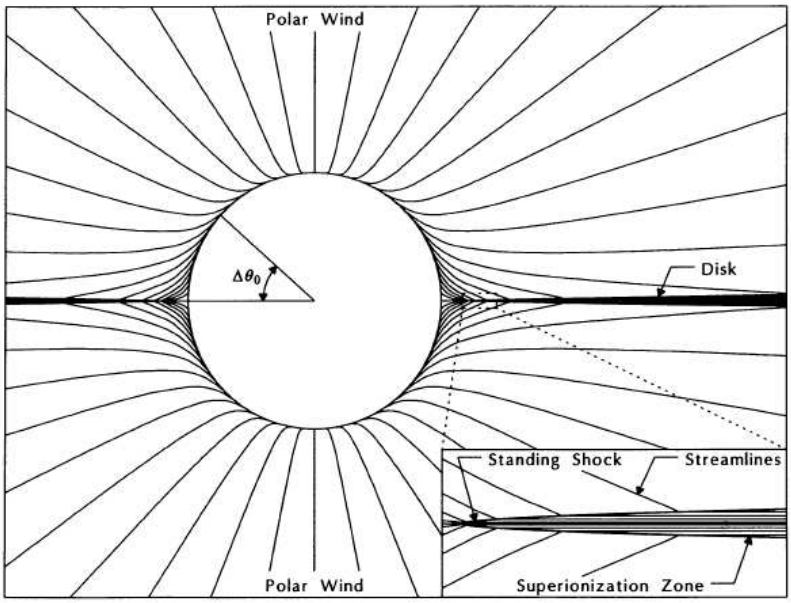

Figure 1.8: Schematic view of the wind-compressed disk model (Bjorkman & Cassinelli 1993). Inset figure represents the shock which turns the flow parallel to the equator prevents the streamlines from crossing at the equator (θ_0 denotes the initial latitude).

1.3.2 Radiatively-Driven Winds (The Wind Compressed Disk Model-WCDM)

The WCDM which is based on rapid rotation and wind streamlines was created by Bjorkman and Cassinelli in 1993. Produced wind streamlines by high rotation from different hemispheres of massive star intersect each other (if rotation is high enough) and they cause a shock at the equator (Figure 1.8). In this scenario "the ram pressure of the wind compresses and confines the equatorial material, and creates a dense equatorial disk (Bjorkman & Cassinelli 1993)".

While numerical hydrodynamic simulations (Owocki et al. 1994 & 1996) are consistent with the model, some physical parameters in these simulations belonging to the disk are not matched up to those used in WCDM. In addition to this inconsistency later works show that observed strong IR excess can not be explained by WCDM (Porter 1997).

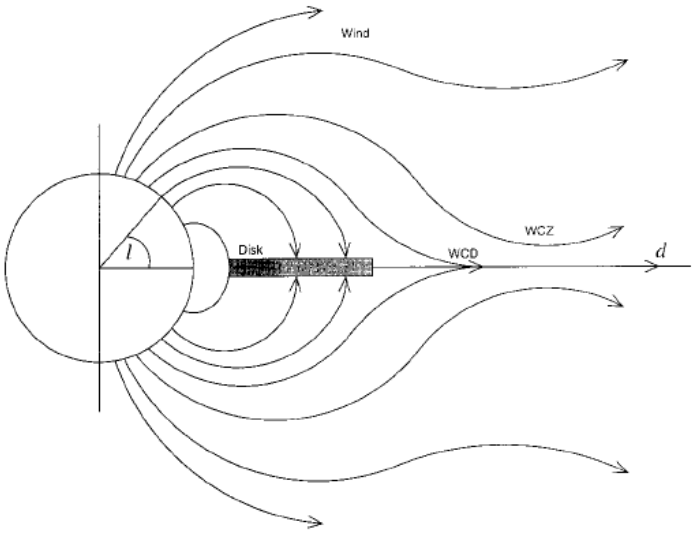

Figure 1.9: Overall structure assumed in magnetically torqued disk model (WCZ denotes wind compressed zone). The star has a dipole-like inner field with axis aligned with the rotation axis of the star. Material leaving the star at latitude l is channeled by the field to the equatorial disk at $r = d(l)$. The rotation causes the channeling process to transfer angular momentum from the star to the disk. This will lead to a distribution of angular speed v_ϕ vs. the equatorial distance d from the star. Note that in the outer regions the field lines are stretched and drawn out by the flow from the star (Cassinelli et al. 2002).

1.3.3 Magnetic Activity (The Magnetically Torqued Disk Model-MTDM)

Despite the lack of convective cells to produce a meaningful magnetic field by dynamo action, according to the MTDM a magnetic field can be generated near the boundaries of convective cores of Be stars (Cassinelli et al. 2002, Charbonneau & MacGregor 2001).

In short, near the equator regions where the magnetic energy dominates over the kinetic energy density, the streamlines (like WCDM) trace the magnetic field lines and force the gas coming from the opposite hemispheres to flow toward

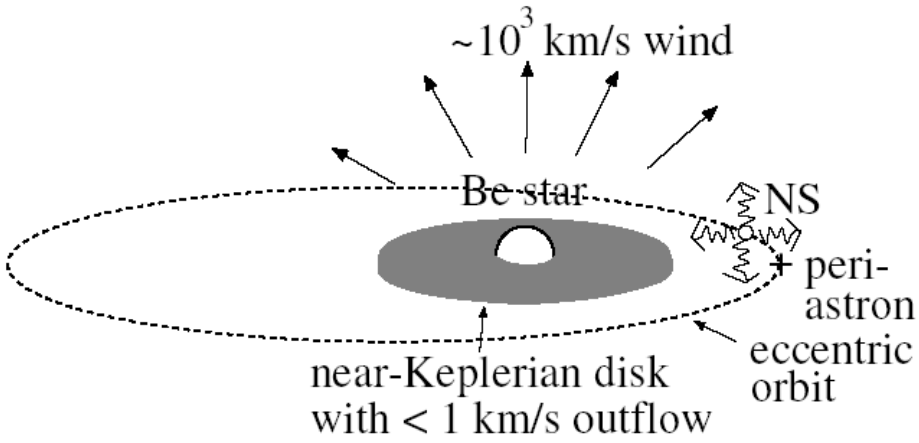

Figure 1.10: Schematic view of a Be/X-ray system (Okazaki & Negueruela 2001)

the equator. Nevertheless a shock region is formed and it creates a dense disk there (Figure 1.9).

While MTDM enables to produce continuum IR excess it is deficient to explain line profile variability seen in the spectrum (Owocki & ud Doula 2003, Porter & Rivinius 2003).

1.3.4 Viscous Decretion Disk Model-VDDM

VDDM which is the most successful and convincing model suggested ever is similar to the viscous accretion disk model except the sign of the mass flow rate (Porter 1999, Okazaki 2001)and it was proposed by Lee et al. in 1991. The model enables to explain the origin of X-ray outburst (Type I and Type II) and the variation of the violet peak (V:short wavelength) and the red peak (R:long wavelength) strengths seen in the case of double-peaked emission line profile. In this model, the main parameter that controls the drifting away of the material from the equatorial regions and producing the disk is the viscosity. The decretion disk of a Be star which is defined as geometrically thin and near Keplerian seen in Figure 1.10 (Okazaki & Negueruela 2001). Contrary to common belief, there is a gap between the disk and the orbit of the NS in the

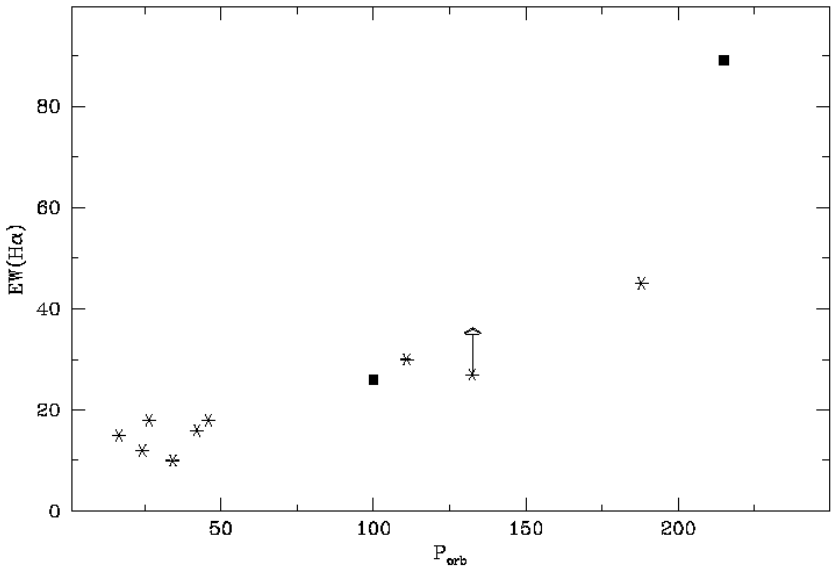

Figure 1.11: Maximum H_α emission as a function of the orbital period. The two systems marked with solid squares have had their orbital period deduced from P_{spin}/P_{orb} diagram(Corbet diagram, Corbet 1986). The arrow represents a lower limit of the H_α equivalent width (Reig et al. 1997).

figure. In other words the NS's orbit never intersects to the middle of the disc.

VDDM has also changed another common belief about the interaction between the decretion disk and the neutron star. It was thought that the interaction worked in only one direction: the disk influenced the NS. However, the correlation between the maximum equivalent width of H_α line and the orbital period (Figure 1.11) shows that this interaction works in both ways that the NS may have some effects on decretion disk such as truncation by resonant/tidal torques (Reig et al. 1997).

In wide orbit systems, the negative tidal torques produced by the NS are limited and disk may extend beyond the *L1* point[2] if the viscosity is high enough. Such systems show regular periodic Type I outbursts. On the other hand for the close systems the truncation of the disk by tidal torques prevents excess of the materials ejected by equator regions to the outer disk boundaries. If the per-

[2]L1: Lagrangian Point 1

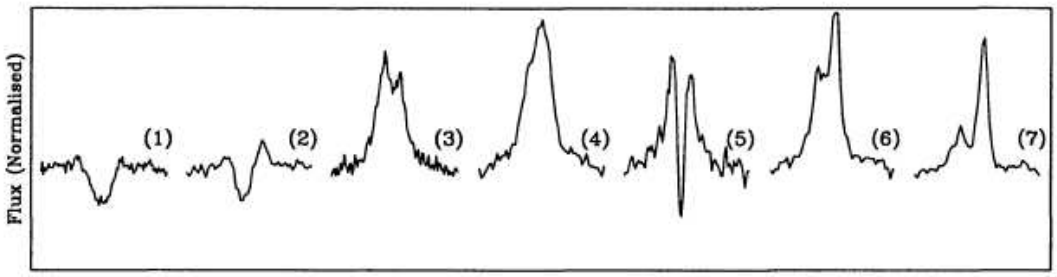

Figure 1.12: Changing of H_α emission line profile for V635 Cas between the years 1995 and 1998 (Negueruela & Okazaki 2000). In the first profile the disk is absent. As the disc appears (2), it quickly grows into a double-peaked (3). Gradually, the peaks converge until a single-peak profile is seen (4), indicating the warping of the disk. A number of fast transitions between single-peaked and shell profiles (5), indicates precession of the warped disc. Finally the disc is very perturbed and the asymmetry grows as the strength of the emission line decreases (6 & 7), leading to a new disc-less phase.

turbation such as a global density wave (main reason of the V/R variations[3]) or radiation-induced warping somehow produce eccentric disk, then material can be accreted through *L1* point (Negueruela & Okazaki 2000). Therefore short and irregular series of Type I outbursts are seen.

In some occasions, the accumulation of the material can make the outer disk sufficiently optically thick. Since the optically disk is unstable, it may warp and precess under the influence of the radiation of Be star (Porter 1998). Precession of the warp disk which lasts weeks to months leads to variations in line profiles seen in the spectrum especially emission lines (Figure 1.12). Due to the fast stellar wind and stellar radiation the warped regions of the disk become deformed and elongated after a while. Therefore large amount of the material flows to the NS and leads to produce Type II outbursts making the disk fainter.

[3]V/R variation: The variation which is seen in the ratio of the violet to red peak in double-peaked emission line profile.

CHAPTER 2

THE SOURCES

In this chapter, the general properties and historical background of the two selected Be/X-ray binary systems are presented: GRO J2058+42 and V0332+53. The main reason of the selection is because of the fact that their optical counterparts show different types of H_α emission line behaviors. In other words, kinematical and geometrical features of their circumstellar disk structures do not have similarities, since emission lines appear in the spectrum contain all these informations.

2.1 The Transient X-ray Source V0332+53 and Its Optical Counterpart BQ Cam

2.1.1 X-ray Outburst Characteristics

The hard X-ray transient V0332+53 (X0331+53) was discovered on June 1, 1973 with the *Vela* 5B satellite during a giant outburst that lasted for about 100 days (Terrell et al. 1983, Terrell & Priedhorsky 1984). The intensity of the outburst reached $\sim$ 1.4 Crab (1.5×10^{38} erg s^{-1}) in the 3-12 keV energy range. This was typically a Type II outburst (Whitlock 1989, Negueruela et al. 1999). During next ten years no significant X-ray radiation belonging to this system was detected.

On November 14, 1983, *Tenma* satellite detected a new outburst of V0332+32

(Tanaka 1983). Actually this outburst was the first of the three small outbursts identified as Type I outbursts, reached 0.06 Crab at its maximum brightness, separated with the orbital period and centered on periastron passage. The outburst series lasted three months and quoted as having unusual properties such as appearance of rapid random fluctuations which was attributed to the magnetized NS (Makishima et al. 1990). Subsequent observations of these outbursts which were carried out by *EXOSAT* (The European Space Agency's X-ray Observatory) revealed the pulsation period, orbital period of the pulsar and eccentricity of the system as 4.37 s, 34.25 days, and 0.31 respectively (Stella & White 1983, Stella 1985).

V0332+53 underwent another outburst which was discovered by the *Ginga* satellite (Takeshima et al. 1994) in September 1989. The analysis of the observation confirmed that it was a giant outburst with a flux of 0.4 Crab in the energy range 1-20 keV. Also a cyclotron resonant scattering feature at 28.5 keV (corresponding to a magnetic field of $\sim 3 \times 10^{12}$ G at the surface of the NS) and quasi-periodic oscillations (QPOs) at 0.051 Hz were found (Makishima et al. 1990, Takeshima et al. 1994).

The last quoted outburst of the source was in 2004 with a peak intensity 1.1 Crab (Type II) in the energy range 1.3-12.1 keV (Remillard 2004, Reig et al. 2006). Kreykenbohm et al. announced the observed three cyclotron lines using *INTEGRAL* (The International Gamma-Ray Astrophysics Laboratory) in 2005, while Que et al. (2005) reported the new QPO at 0.22 Hz using *RXTE* (The Rossi X-ray Timing Explorer) observations.

2.1.2 Optical Counterpart: BQ Cam

In addition to the orbital parameters, analysis of the outburst series mentioned above led optical counterpart of V0332+53 to be discovered (Bernacca 1983, Bernacca et al. 1984, Stocke et al. 1985, Honeycutt & Schkegel 1985, Stella 1985). Bernacca et al. (1984) remarked that the probable companion of the NS was a star of magnitudes V=15.13±0.03 and B-V=2.31±0.04. He also declared

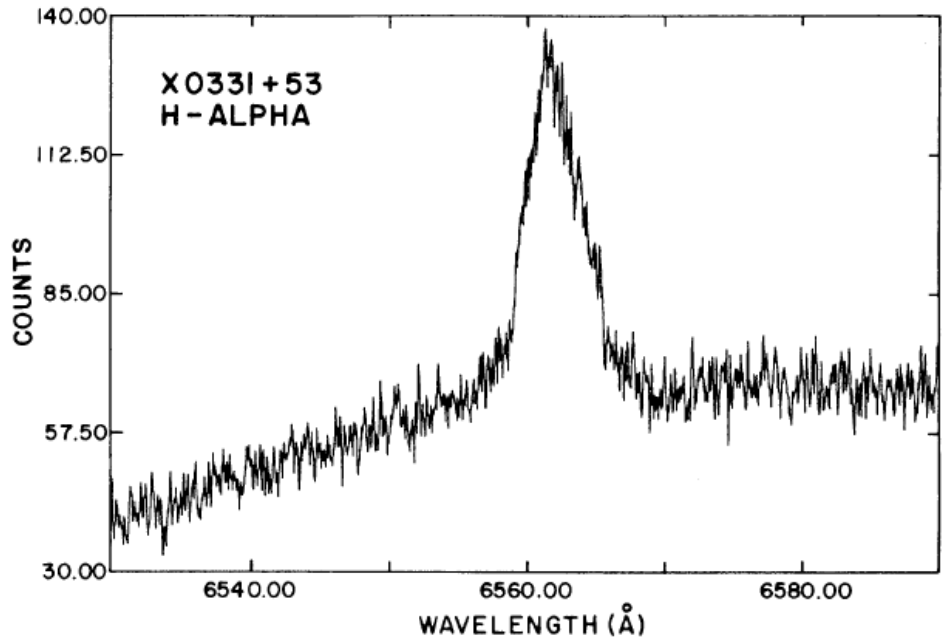

Figure 2.1: A high-resolution profile of H_α in optical candidate of V0332+53 (X0331+53) taken with the MMT (Multiple Mirror Telescope) echelle spectrograph in late January 1984 (Stocke et al. 1985).

that H_α (λ6562.8 Å) line appeared in emission in the spectrum having P-Cygni profile with the absorption component and determined it as a heavily reddened Be type star.

Afterwards, using spectrophotometrical results, Honeycutt and Schlegel (1985) determined the probable counterpart to V0332+53 as an OB star, with the color B-V=1.62±0.06, extinction E_{B-V}=1.93±0.06 and with the magnitudes of B=17.04 and V=15.42. However calculated magnitudes belonging to the optical companion were rather different from those of Bernacca et al. (1984). Honeycutt and Schlegel (1985) attributed these difference to the IR variations of the star which were mentioned before by Williams et al. (1983) and reflection effects of accretion disk that made the source appear more bright or faint. They also reported the weak emission of H_β (λ4861.3 Å), H_γ (λ4340.5 Å) and absorption of HeI λ4471 line.

Later works, except HeI λ4471 line, the existence of H_α (Figure 2.1) emission

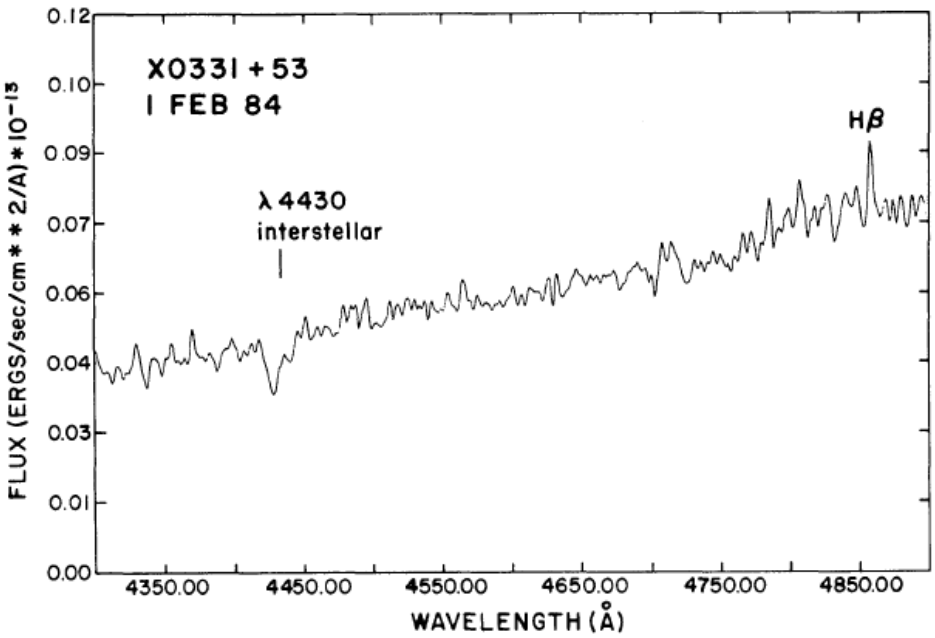

Figure 2.2: A 1Å resolution spectrum of the blue region of BQ Cam taken on 1984 February 1 with the MMT spectrograph (Stocke et al. 1985). Strong diffuse interstellar band (DIB) at λ4430 and weak H_β emission are clearly visible, while HeI λ4471 is absent opposite to the results of Honeycutt & Schlegel (1985).

line (however without the P-Cygni profile) and the other observed emission features appeared at H_β and H_γ (Figure 2.2) wavelengths were confirmed by Stocke et al. (1985) using high resolution spectroscopy. He interpreted the absence of the photospheric absorption line as the sign of the optical continuum which did not arise close to the primary star.

Using medium dispersion optical spectroscopy, Corbet et al. (1985) represented that the equivalent width (EW) of the H_α emission line in the spectrum showed a decrease by a factor of $\sim$2 (measured EW=5.9$\pm$0.6 Å) compared with previous results. They determined the probable reason of this decrease as the existence of a evolving circumstellar disk taking place around BQ Cam. Examining both photometric and spectroscopic results they also obtained $V \sin(i)$=150 Km s^{-1} and they also added that the source was viewed at low i (assuming i$<$15°) due to the observed single-peaked H_α emission (See Struve model in

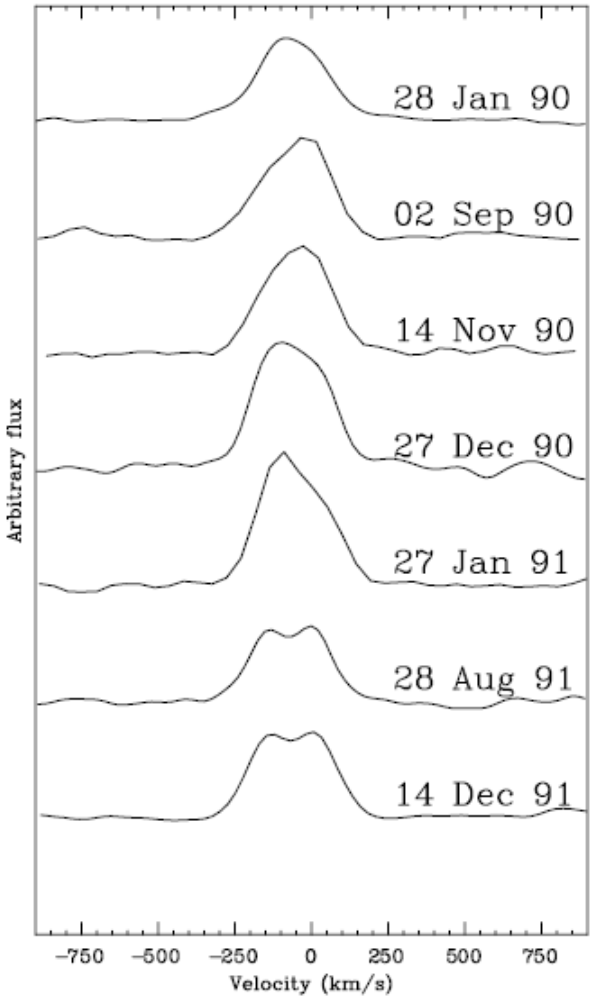

Figure 2.3: H_α observations of BQ Cam during the period 1990-1991 (Negueruela et al. 1998).

Chapter 1.3.1).

The H_α observations of BQ Cam between 1990-1991 (Negueruela et al. 1998) showed the existence of V/R variability (with a quasi-period of $\sim$ 1 year) which is an indication of the propagation of the density wave in the disc (Figure 2.3). They also noted the disappearance of the observed V/R variability by 1992. Unfortunately there were no significant photometric or spectroscopic observations of BQ Cam up until 1997. Thus the evolution of the disc remained quite unclear between these years. The Figure 2.4 represents the last published emission profiles of the source seen in the spectrum performed by Negueruela et al.

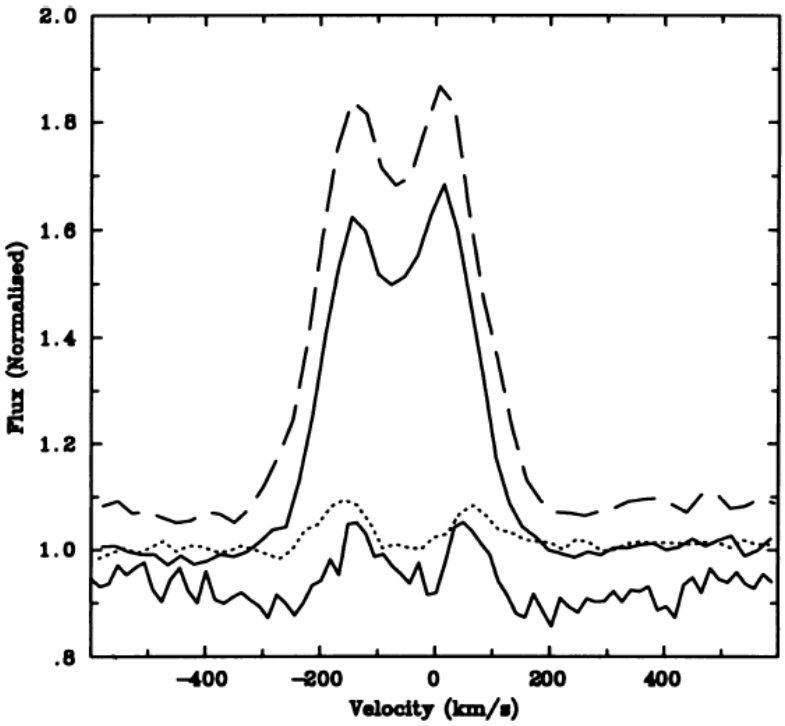

Figure 2.4: Emission lines in BQ spectrum observed on 1997 November 14 (Negueruela et al. 1999). From bottom to top, H_β, HeI λ6678 (dotted line) and H_α . Dashed lines represent the H_α line observed on 1991 December 12.

(1999). They also determined BQ Cam as a O8-9Ve type star at a distance of $\approx$ 7 kpc based upon their photometric and spectroscopic results.

2.2 The Be/X-ray Binary System GRO J2058+42

GRO J2058+42, a transient 198 s X-ray pulsar, was discovered by *BATSE* (Burst And Transient Source Experiment) instrument of *CGRO* (Compton Gamma Ray Observatory) in September 1995 during its Type II outburst of which flux reached to a peak value of 130 mCrab in the 20-50 keV energy range (Wilson et al. 1995). After this giant outburst, five small outbursts were detected with the mean peak flux of 15-20 mCrab in the 20-50 keV band by BATSE as well. The outbursts, each lasted about two weeks, were separated with 110 days (Wilson et al. 1996). Then the optical period of the source was determined

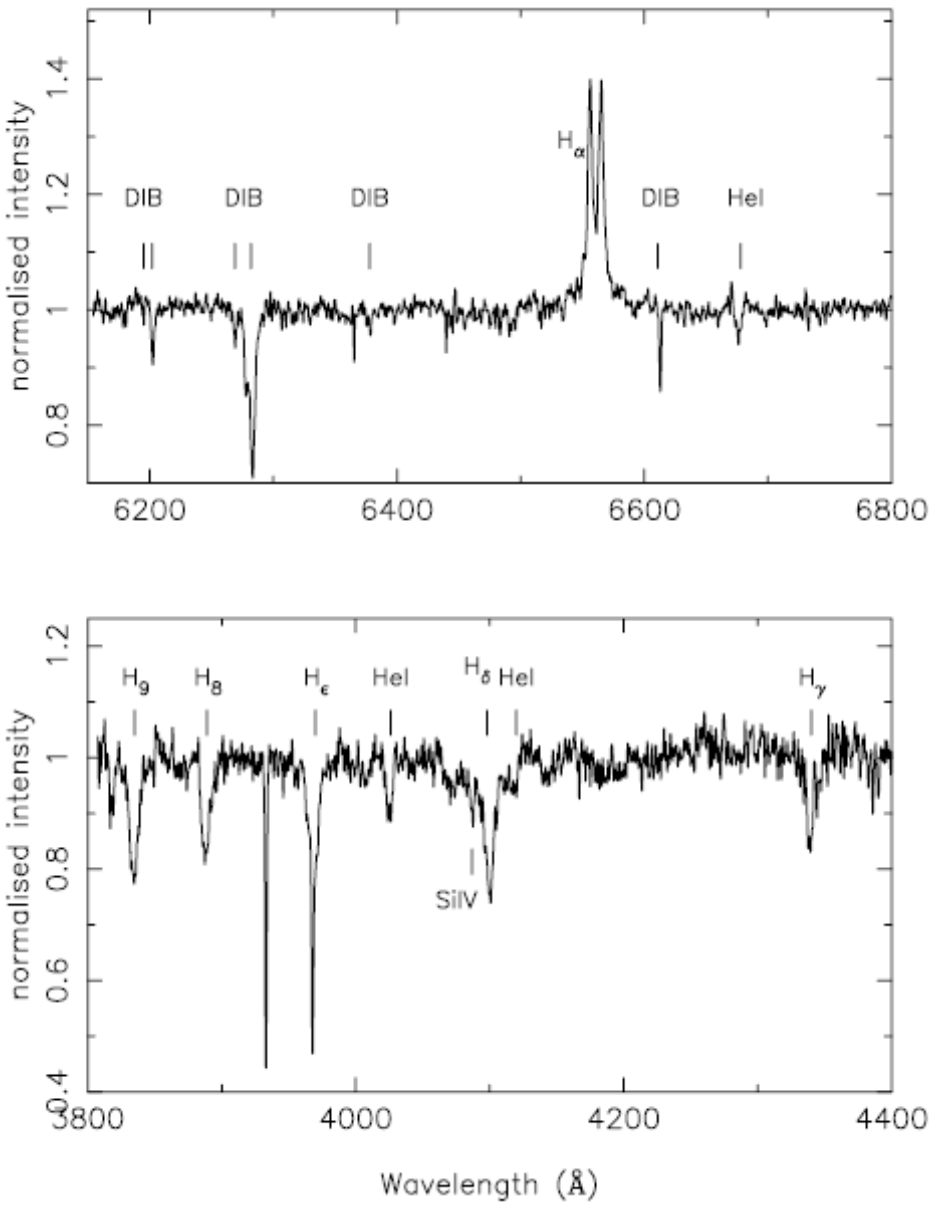

Figure 2.5: Red(top) and blue(bottom) spectrum of the counterpart to CXOU J205847.5+414637 which was taken on 2004 July 4 (Wilson et al. 2005). A strong H_α profile, HeI λ6678 and various DIBs are visible. In the blue, several lines from the Balmer series, the HeI lines at $\lambda\lambda$4026, 4121 Å and SiIV 4089 Å can be seen in absorption.

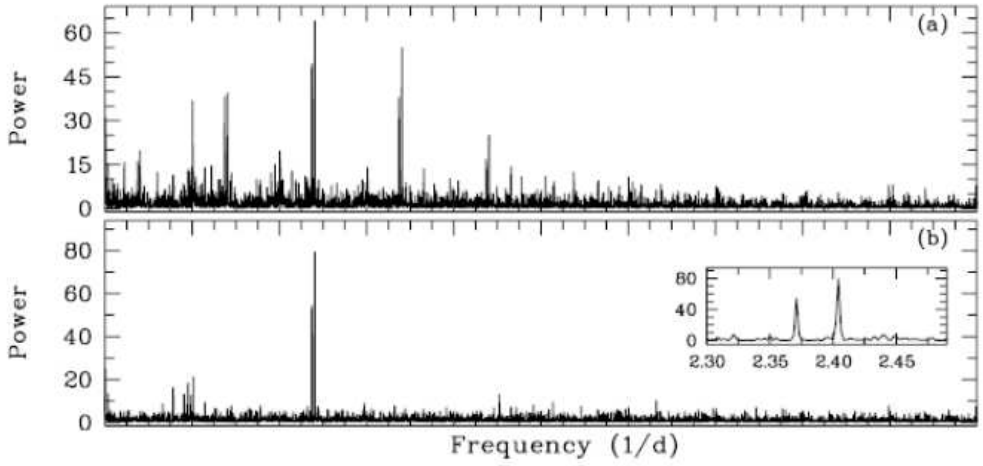

Figure 2.6: Power spectra for the optical counterpart to GRO J2058+42 (Kızıloğlu et al. 2007). Panel **a**) Lomb-Scargle algorithm; **b**) Clean algorithm. Frequencies at 2.404 and 2.371 d^{-1} are shown in the inset of the middle panel for clarity.

as 54 days (Corbet et al. 1997) by analyzing the *RXTE ASM* (All-Sky Monitor) data which were taken between January 1996 and 1997. Although GRO J2058+42 was thought to be as a Be/X-ray binary, depending on estimated P_{spin} and P_{orb} values, no optical counterpart was proposed until 2004.

Using GRO positions Reig et al. (2004) announced the probable optical counterpart to the source as a star having double-peaked H_α emission line with a mean EW of 4.5 Å which was located at $\alpha = 20^h58^m47^s$, $\delta = +41°46'36''$ with the magnitudes of B=16.04, V=14.92, R=14.23 and I=13.49. However further *Chandra* observations did not confirm the existence of a source inside the CGRO error circle, except CXOU J205847.5+414637 which was located just outside the circle. Later with the help of the optical and spectroscopic observations obtained by Wilson et al. (2005), it was understood that CXOU J205847.5+414637 showing H_α emission in it spectrum (Figure 2.5) was the same object as the one proposed by Reig et al (2004). They determined the spectral type and the luminosity class of the counterpart of GRO J2058+42 as

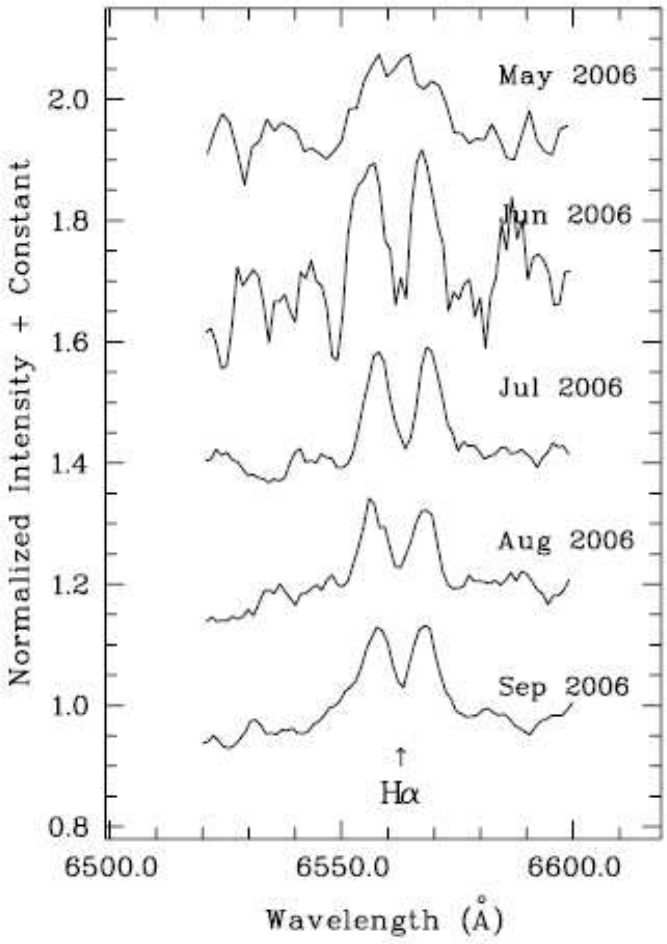

Figure 2.7: H_α profiles, observed May-September 2006, belonging to optical companion of CXOU J205847.5+414637 (Kızıloğlu et al. 2007).

O9.5-B0IV-V.

Long-term optical monitoring of the system between 2005 and 2006 performed with ROTSEIIId (Robotical Optical Transient Experiment) and optical spectroscopic observations obtained with RTT150 revealed another behavior of the system (Kızıloğlu et al. 2007). These observations showed that the system had a NRP with the frequency of 2.404 d^{-1} connecting with the short-term variability (Figure 2.6). The absence of the outbursts from 2002 to that day was interpreted as the stability of the inner part of the disk by Kızıloğlu et al. (2007). Also the results of their spectroscopic observations which showed H_α emission line confirmed the existence of the disk during its quiescent phase

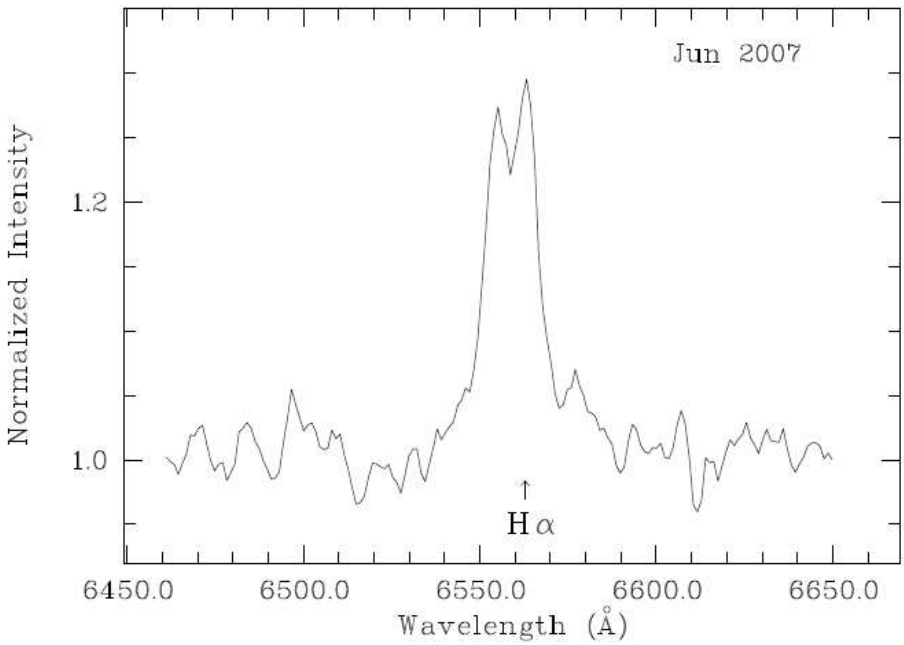

Figure 2.8: H_α profile of the source with the EW of 5.4 Å, performed by Kızıloğlu et al. (2008a), observed on 2007 June 14.

Figure 2.7.

After an optical brightening about 0.3 mag and enhancement at the EW of H_α emission ($EW_{H\alpha}$=5.4 Å) detected in the system (Kızıloğlu et al. 2008a), GRO J2058+42 ceased its quiescence phase undergoing a new small X-ray outburst in May 2008 (Krimm et al. 2008, Kızıloğlu et al. 2008b). It was the first outburst of the system detected during last six years. The enhancement at the EW of H_α emission line profile which is the sign of the last observed X-ray activity seen in Figure 2.8.

CHAPTER 3

OBSERVATION AND DATA REDUCTION

3.1 Optical Observations

The spectroscopic and photometric observations of optical the counterpart of V0332+53 and GRO J2058+42 were obtained with medium-resolution spectrometer TFOSC[1] which is mounted on RTT150, located at TUG[2], Antalya, Turkey. The optical bench of the instrument consists of a collimator existing behind the aperture wheel and a Fairchild 447BI CCD camera having a field of view (FOV) 13.3′, equipped with 2048 × 2048, 15 μ pixel (0.39″ pixel^{-1}) chip. Since having a filter wheel (with 12 filter holders) and a grism wheel (with 9 different types of grism) separately, both imaging and spectroscopy can be performed one after the other.

During the spectroscopic observations of the sources, grisms G7, G8, G14 and G15 were used whenever needed. For the H_α profile analysis usually G8 was used because of its sensitivity. It is sensitive in the wavelength range 5800-8300 Å with the average dispersion ∼1.1 Å pixel^{-1}. The spectral ranges and the average dispersions of the other grisms are 3850-6850 Å with ∼1.5 Å pixel^{-1}

[1]TFOSC (TUG Faint Object Spectrometer) is the last one of the FOSC (Faint Object Spectrograph and Camera) series produced by Copenhagen University Observatory (CUO).

[2]TUG: TÜBITAK National Observatory

http://www.tug.tubitak.gov.tr

Table 3.1: Journal of spectroscopic observations of optical counterpart to GRO J2058+42.

Date	MJD[a]	Grism	Exp. (s)	Slit (μ)
2006 May 23	53878	G7	4×600	54
2006 July 29	53945	G7	2×1200	54
		G8	2×1800	54
		G15	1800	54
2006 August 19	53966	G8	1800	67
		G14	1800	67
2006 September 26	54004	G8	1800	67
		G14	3600	67
2007 June 14	54265	G8	2400	67
2007 December 14	54448	G8	2400	67
2007 December 19	54453	G8	2400	67
2008 May 12	54598	G8	2400	67
2008 June 19	54636	G8	2400	67

[a]Modified Julian Date = JD (Julian Date)- 2400000.5

for G7, 3275-6100 Å with ∼1.4 Å pixel^{-1} for G14 and 3300-9000 Å with ∼3 Å pixel^{-1} for G15.

Details of the optical spectroscopic observations of the sources are presented in Table 3.1 and Table 3.2. It should be also pointed out that we have low signal-to-noise ratio (SNR) for May and June 2006 observations of the system GRO J2058+42 due to the problems with the autoguider.

In addition to the standard observations , we also observed two spectrophotometric standard stars BD+25 3941 and HILTNER 102 to compare the spectra of the optical counterparts of V0332+53 and GRO J2058+42. HILTNER 102 is an O9.7 II type star (Unger et al. 1998) with the magnitudes of B=11.10 and

Table 3.2: Journal of spectroscopic observations of BQ Cam.

Date	MJD	Grism	Exp. (s)	Slit (μ)
2006 September 26	54004	G8	1800	67
2006 December 23	54092	G8	1800	67
2007 January 23	54154	G8	1800	67
2007 April 07	54197	G8	2400	67
2007 July 18	54300	G8	2400	67
2007 July 19	54301	G8	1800	67
2007 September 13	54357	G8	2400	67
2007 October 05	54378.86	G8	1800	67
	54379.07	G8	1800	67
2007 December 14	54448	G8	2400	67

Table 3.3: Journal of spectrophotometric standard stars.

Star*	Date	MJD	Grism	Exp. (s)	Slit (μ)
Star 1	2006 July 29	53945	G7	900	54
			G8	900	54
Star 2	2007 June 15	54266	G8	600	67
			G14	1200	67

* Star1 and Star 2 represent BD+25 3941 and HILTNER 102 respectively.

V=10.42, the other standard star BD+ 25 3941 is a main sequence B1.5 type star with the magnitudes of B=11.03 and V=10.47. Journal of the observations of the standard stars is represented in the Table 3.3.

Despite the fact that analyzing the Hα line profiles is our main aim, we also took the image of the counterparts with different filters (B, V, and R) to estimate

the amount of their extinctions and distances. The journal of photometric observations, performed through the B,V and R filters, are presented in Table 3.4 and 3.5.

Table 3.4: Journal of photometric observations of optical counterpart to GRO J2058+42.

Date	MJD	Filter	Exp. (s)
2006 May 24	53879	R	3×30
2006 June 16	53902	R	3×40
2006 July 29	53945	B	2×120
		R	2×40
2006 August 19	53966	R	4×40
2006 August 21	53968	R	3×5
		R	2×30
2006 September 26	54004	R	4×40
2007 June 14	54265	B	2×60
2007 December 14	54448	R	3×30
		B	60
2007 December 19	54453	R	30
2008 May 12	54598	R	2×30
		B	2×60
2008 June 19	54636	R	2×30
		B	30

Table 3.5: Journal of photometric observations of BQ Cam.

Date	MJD	Filter	Exp. (s)
2006 September 26	54004	R	2×40
2006 December 23	54092	R	2×30
2007 January 23	54154	R	30
		V	2×60
		B	120
2007 April 07	54197	R	3×30
		V	3×60
		B	3×120
2007 July 18	54300	R	2×30
		V	60
		B	120
2007 July 19	54301	R	2×10
2007 September 13	54357	R	4×10
		V	30
		B	60
2007 October 05	54378	R	3×30
		V	60
		B	120
2007 December 14	54448	R	30
		V	60
		B	120

Table 3.6: Accurate coordinates and magnitudes of GRO J2058+42 and photometric reference stars.

Star	α(J2000)	β(J2000)	B^a	R^a
J2058+42	$20^h58^m47^s.54$	$+41°46'37''.3$	16.70	13.39
Star 1	$20^h58^m57^s.99$	$+41°47'26''.5$	13.78	12.03
Star 2	$20^h58^m41^s.54$	$+41°47'20''.8$	17.22	14.11

[a]B and R magnitudes are obtained from USNO B1.0 Catalogue.

3.2 Data Reduction

The reduction and analysis of the spectrums were made using the packages Longslit context and Echelle context of MIDAS[3]. After applying standard reduction process (bias substraction and flat fielding) to the spectrums we used the command "FILTER/COSMICS" whenever needed to remove the unwanted saturated pixels occurring due to the cosmic rays. The lines in both source spectrum and the spectral lamp spectrum were extracted with "EXTRACT/LONG" and "SEARCH/LONG". Fe-Ar (Iron-Argon), He (Helium), Ne (Neon) lambs were the spectral lambs that usually used to identify the lines presented in the spectrum of the sources. Then a dispersion relation was applied to the 1D (one dimensional) spectrum by the command of "APPLY/DISPERSION" was used. Since investigating the H_α line profile in the spectrum was our main purpose we did not observe the standard stars at each observation night to flux calibrate spectroscopic data. Instead of flux calibration, we normalized the continuum to unity by dividing the observed spectrum by a smooth approximation of its continuum[2] using "NORMALISE/SPEC". Applying Gaussian fitting to the emission features the FWHM and EW values were obtained from ALICE context of MIDAS. Also Barycentric corrections applied to the spectrums to get the correct velocity estimation.

After standard photometrical reduction procedure the B,V and R magni-

[3]http://www.eso.org/projects/esomidas/

Table 3.7: Accurate coordinates and magnitudes of BQ Cam and photometric reference stars.

Star	α(J2000)	β(J2000)	B^a	V^a	R^b
BQ Cam	$03^h34^m59^s.9$	$+53°10'23''.6$	16.58	11.30	14.37
Star 1	$03^h34^m48^s.8$	$+53°09'33''$	17.17	15.79	15.13
Star 2	$03^h34^m36^s.6$	$+53°10'24''$	17.01	15.59	14.72

[a]B and V magnitudes are obtained from USNO A2.0 Catalogue.

[b]R magnitudes are obtained from USNO B1.0 Catalogue.

tudes of the sources were obtained using SExtractor[4] (Source-Extractor). PSF (Point Spread Function) Photometry were carried out for each corrected image to get the instrumental magnitudes. The calibration of the magnitudes was done by comparing the magnitudes of the reference stars which were obtained from USNO A2.0 R-band and USNO B1.0 catalogues. The selected reference stars for BQ Cam which were in the same frame with the source were also standard stars (Table 3.6). However there were not any standard stars which taken place in GRO J2058+42 frame. For that reason we chose the reference stars as brighter than GRO J2058+42 and placing vicinity of it (Table 3.7). After the calibration step, the airmass calculation was also done for each frame.

[4]http://terapix.iap.fr/soft/sextractor/

CHAPTER 4

OBSERVATIONAL RESULTS AND DISCUSSION

4.1 Counterpart to GRO J2058+42

4.1.1 Line Identification

As seen from observation journals (Pages 27,28,29 and 30), we have nine spectra of counterpart to GRO J2058+42 extending over two years. However it should be pointed out that we observed the optical counterpart of the system when the system was onset of its last X-ray activity (May 2008). The long-term optical light curve of the source which is obtained using ROTSEIIId[1]archive is presented in Figure 4.1 (provided by Prof Dr. Ümit Kızıloğlu).

Since the emission lines in the spectrum (mostly the Balmer lines) are the evidences of circumstellar disk as mentioned previous chapters (Chapter 1.2 and 1.3), the measurements of these lines are generally used to estimate physical and structural parameters of the disk. For that reason we took the broad-band low-resolution spectrum of the source with grism G15 (sensitive in λ3300-9000 Å) to investigate the Balmer lines. Figure 4.2 shows the both broadband and moderate resolution spectra which are taken with grisms G15 and G8 respectively.

[1]ROTSEIIId: Robotic Optical Transient Experiment
http://www.rotse.net/

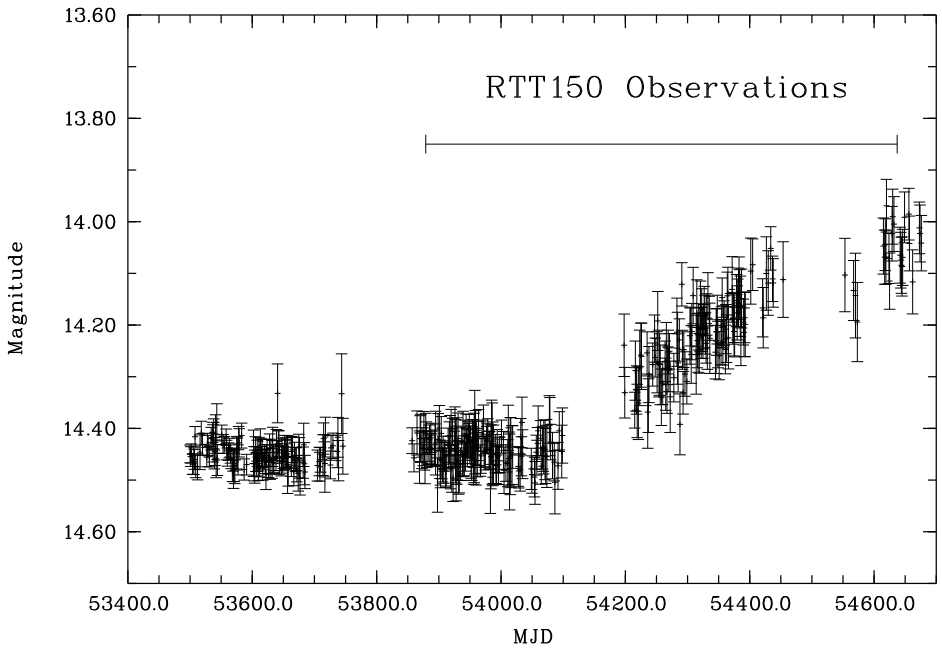

Figure 4.1: Light curve of optical counterpart to GRO J2058+42 obtained by using ROTSEIIId archive. Time of our observations (spectroscopic and photometric) is also remarked with long bar.

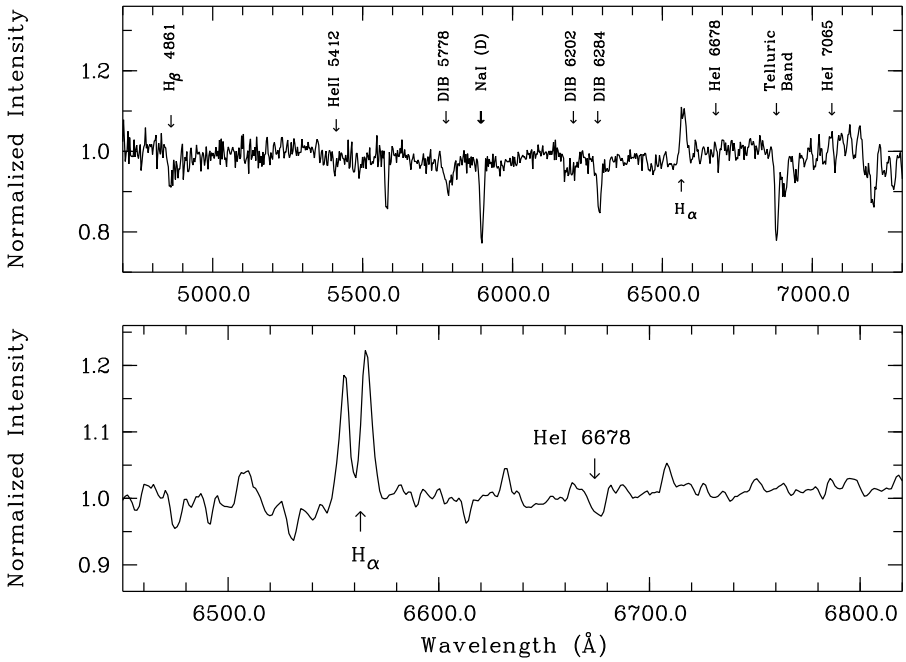

Figure 4.2: Broadband (with G15) and moderate resolution spectra of counterpart to GRO J2058+42 taken in July 2006.

The blue range of the spectrum and the lines take part in it presented in Figure 4.2 and Figure 4.3. In these figures we can see the following features;

a) HeII $\lambda\lambda$4541,4686 and 5412 lines are present and they show clearly absorptions.

   We should like to point out that due to the absence of HeII lines and the lack of information above λ4400 Å in their spectrum, Wilson et al.(2005) classified the optical counterpart of GRO J2058+42 as O9.5-B0 type. Since HeII lines are the noticable features throughout O type region, they might be a indicator of being earlier than B0 type.

b) In contrast to HeI $\lambda\lambda$4026,4121,4144,4387 and 4471 lines which are appeared in early-type spectra, HeI $\lambda\lambda$6678 and 7065 lines are seen as double-peaked with deep central absorptions. The other HeI lines at $\lambda\lambda$4713,4922,5016 and 5048 indicate weak absorption features also.

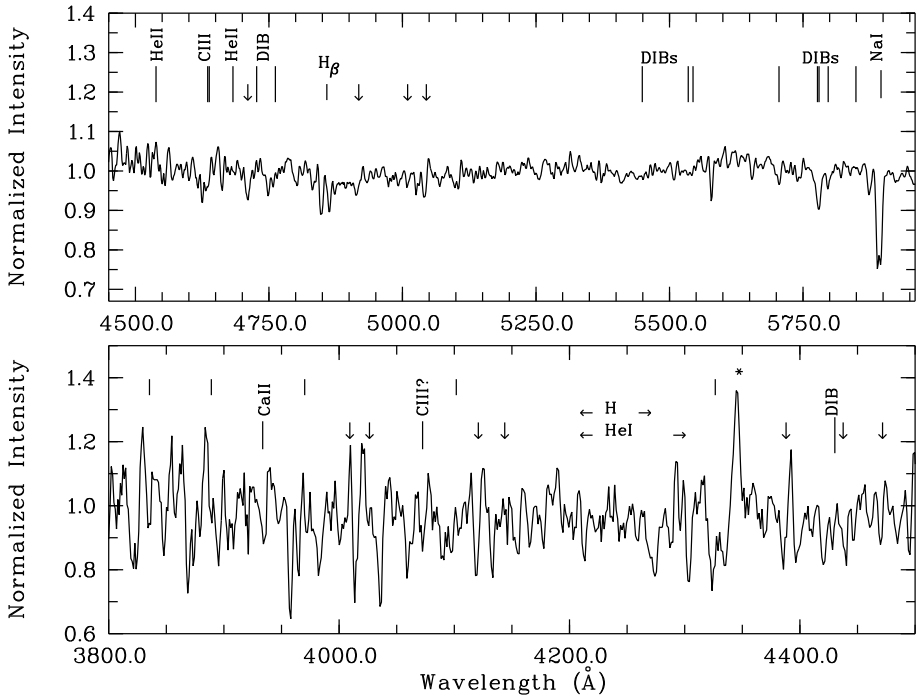

Figure 4.3: Mid band (top) and blue (bottom) spectra of the optical counterpart of GRO J2058+42 taken in July 2006 with G7 and in August 2006 with G14. The Balmer lines, HeI lines and cosmic rays are denoted by short vertical bars, down arrows and stars (*) respectively. DIBs and several other lines are also remarked in the spectra.

c) H_α lines appear in double-peak emission with central absorption which do not reach the continuum level while the majority of the Balmer series lines such as H_β, H_γ, H_δ, H_ϵ, H_8 and H_9 seen in absorption.

d) In addition to CIII lines which appear in weak absorption, CaII λ3934 line which is an indicator of chromospheric activity shows absorption in the blue range of the spectrum (Fig. 4.3).

e) Several DIB features are recognized clearly in blue,mid and broad band spectra.

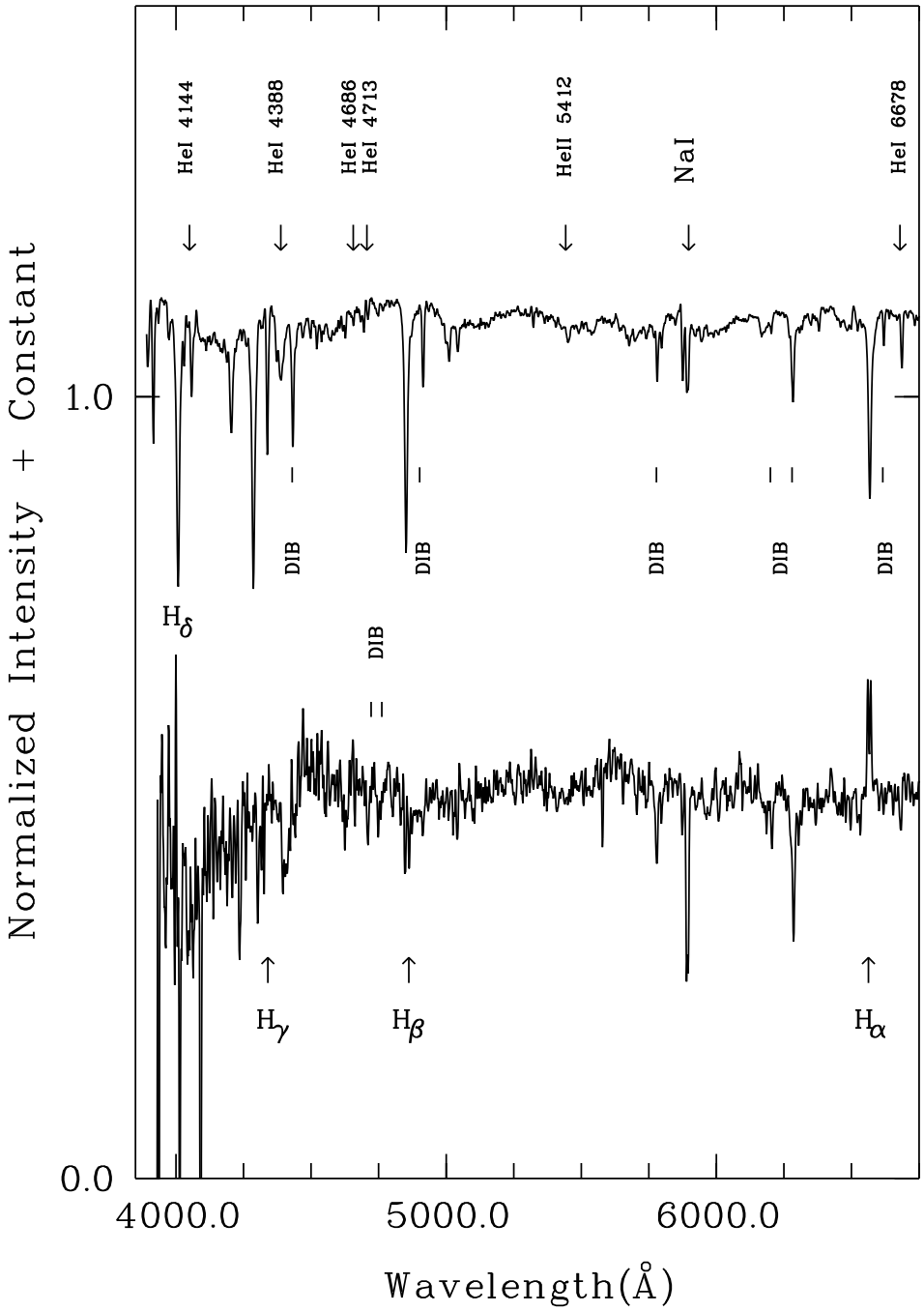

Figure 4.4: The comparison of GRO J2058+42 mid-band (with G7) spectrum (bottom) with the standard star BD+25 3941 spectrum taken in July 2006.

4.1.2 Comparison with Standard Star Spectrum

The comparison of the spectra of counterpart to GRO J2058+42 with standard star BD+25 3941 is represented in Fig 4.4. As we expected the Balmer lines (in absorption) and neutral Helium lines are the most prominent features in the spectrum since BD+25 3941 is a main sequence star with the spectral type of B1.5. Hβ, Hγ and Hδ lines are seen clearly in contrast to Be star spectrum. On the other hand, the NaI λ5896 Å line in GRO J2058+42 is stronger than standard star spectrum.

4.1.3 H_α Line and V/R Variability

It is clear that the strongest feature in the spectra of the optical counterpart of GRO J2058+42 is the H_α emission line. Although the profile shape and its measurements show variations during the period covered our observations, it is always seen in emission (Figure 4.5). A small segment of each spectrum (taken with G8 except May 2006) in λ6400-6700 Å range is also presented in Fig 4.6, 4.7 and 4.8.

Table 4.1 represents EW, FWHM, VSin(i) and ΔV (peak separation) measurements of H_α emission line. The projected rotational velocity values are obtained using the approximation of Buscombe (1969). Applying our mean values for Vsin(i)=357.67±67 km s^{-1} and ΔV=394.39 km s^{-1} to Huang's law (1972),

$$\frac{R_e}{R_*} = \left(\frac{2V\sin(i)}{\Delta V}\right)^2 \tag{4.1}$$

where R_e is the radius of the emission disk and R_* is the photospheric radius of the star. The radius of the H_α emitting region have been found as $R_e = 4R_*$.

The mean EW value of H_α emission line is 2.46±0.17 Å with the peak separation of 454.22±48 km s^{-1} between July-September 2006. The May 2006 values were ignored because of the low SNR value. Next three observations (June-December 2007) shows that the mean EW reaches a value of 5.59±0.38 Å which is roughly two times bigger than the previous ones (Chapter 2.2). Not

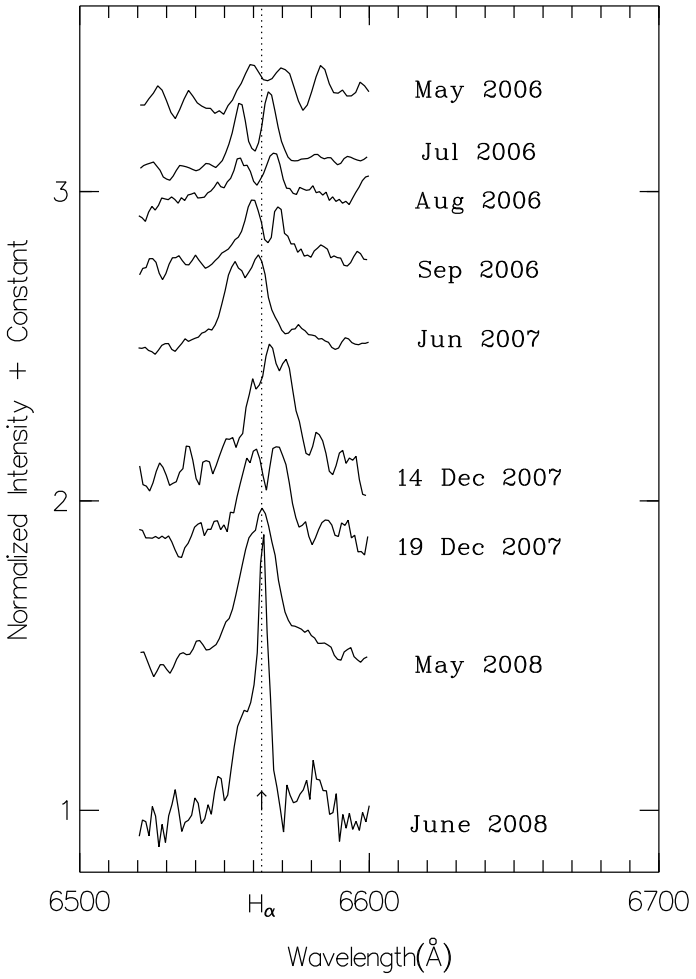

Figure 4.5: Evolution of the H_α profiles observed May 2006-June 2008. Note the low SNR for May 2006 and December 14, 2007 data. Dotted lines represent the laboratory wavelength of H_α line.

only consistent with Kızıloğlu et al. (2008a), but this double EW value also confirms that before the X-ray activity of Be/X-ray binary systems, the EW value of H_α line increases, in addition to optical magnitude of the primary.

The results of May and June 2008 observations are quite important since reflecting the disk structure of the counterpart at the outburst time. Both H_α profile shapes and the EW values show variation during and after the last outburst of the system. H_α emission profile changes as double-peaked to single-

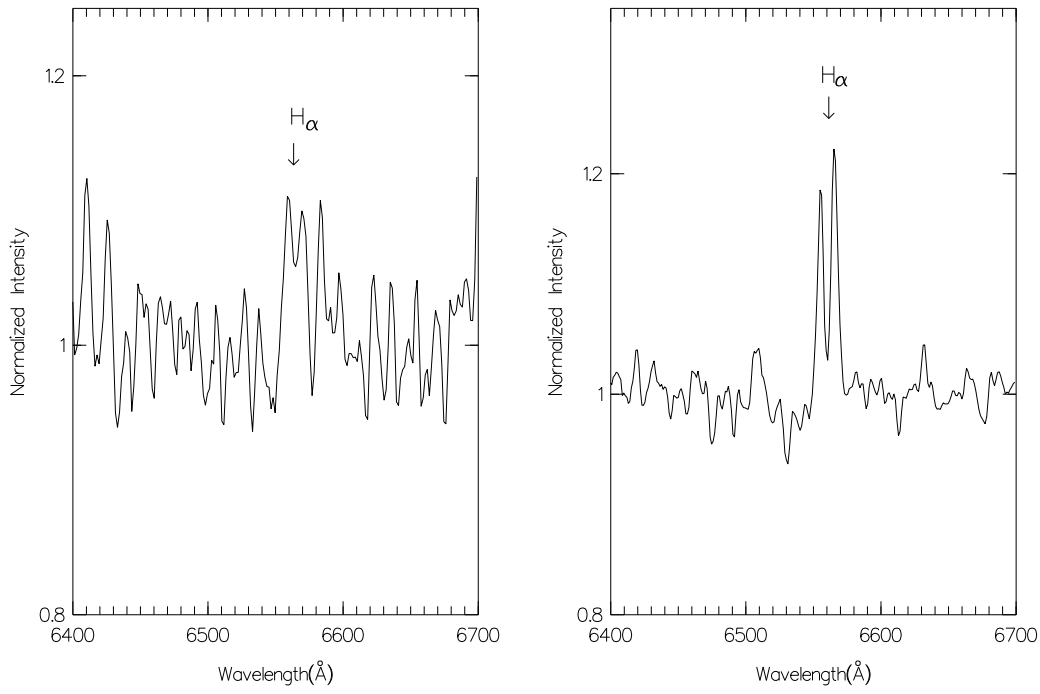

(a) (b)

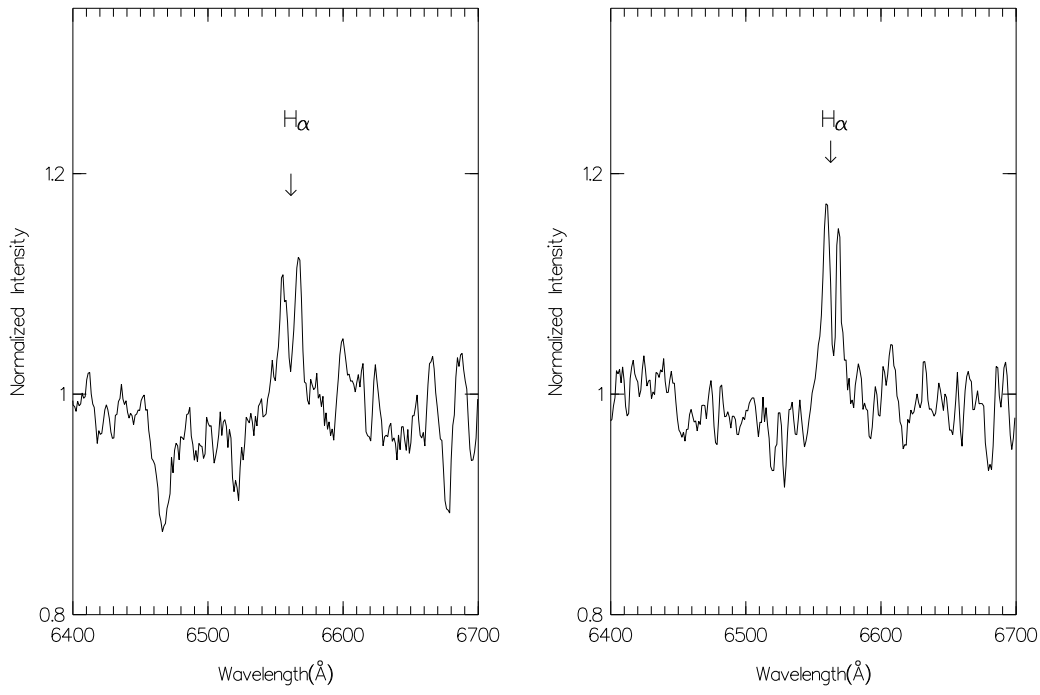

(c) (d)

Figure 4.6: H_α profiles of counterpart to GRO J2058+42 observed in a)May, b)July, c)August and d)September 2006.

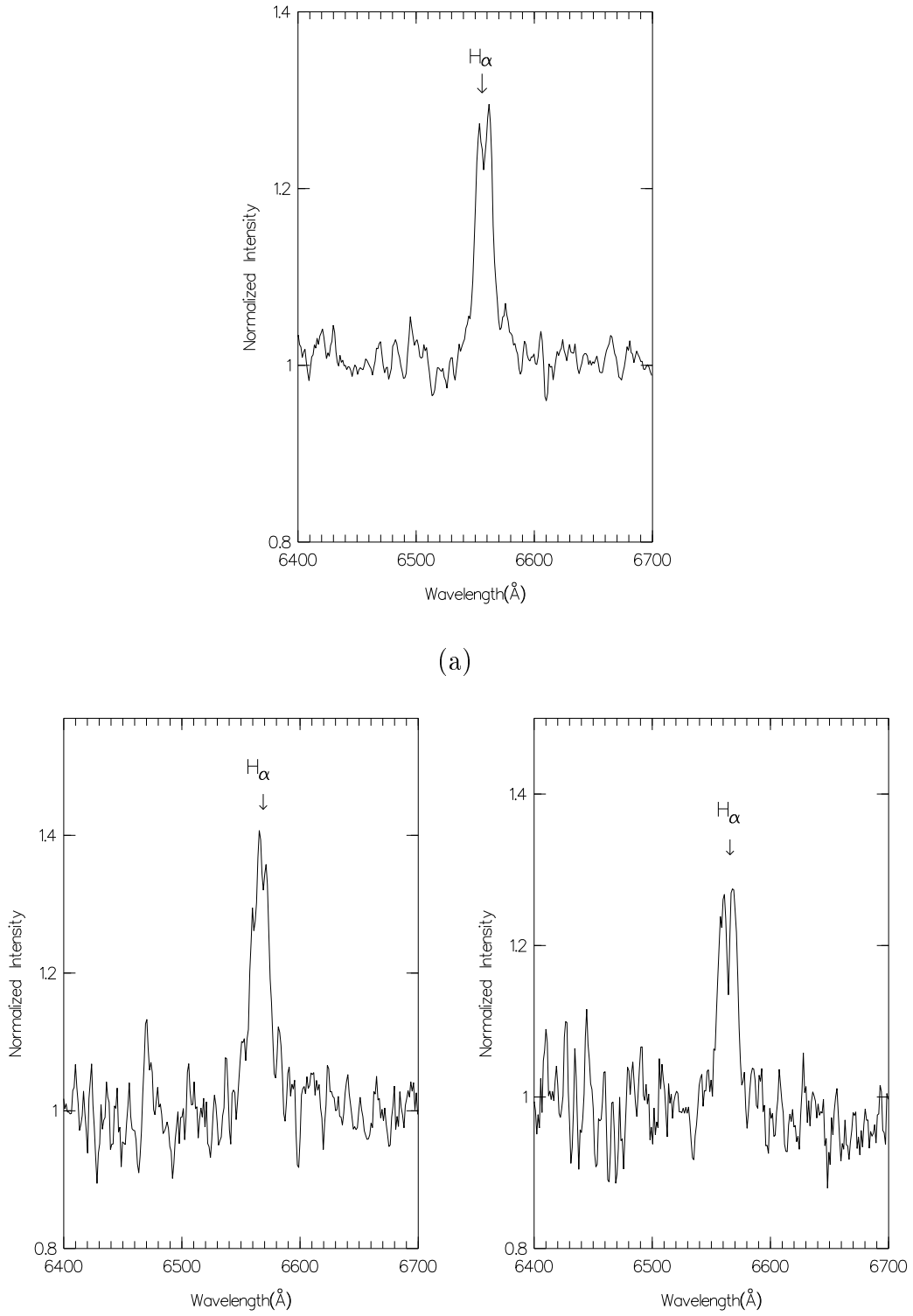

Figure 4.7: H_α profiles of counterpart to GRO J2058+42 observed in a)June 2007, on b)14 December and c)19 December 2008.

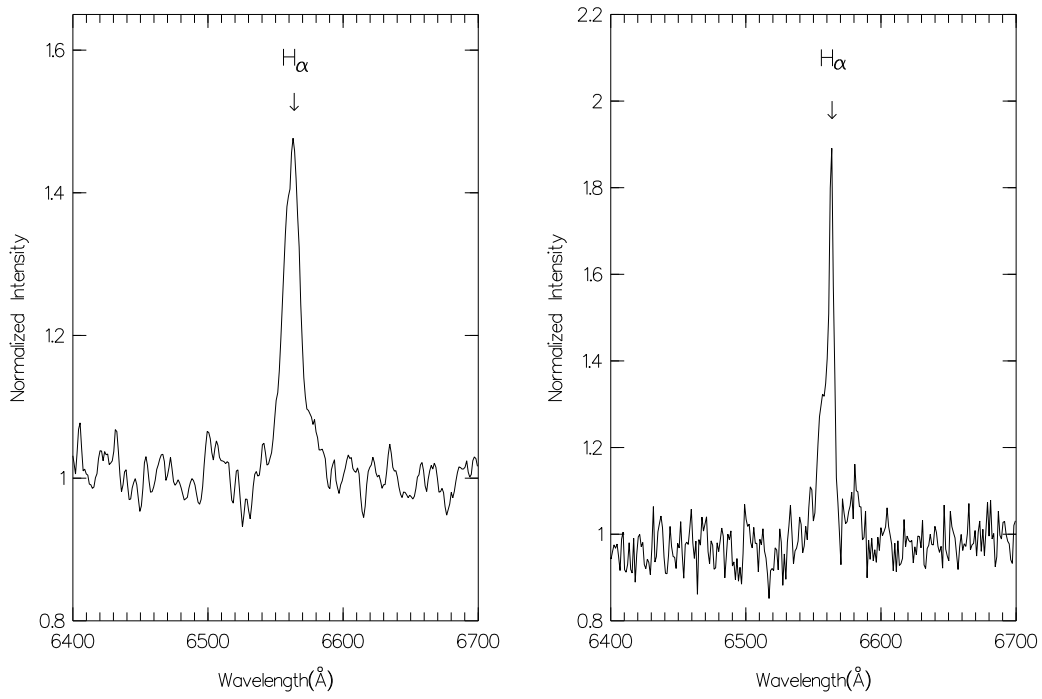

(a) (b)

Figure 4.8: H_α profiles of counterpart to GRO J2058+42 observed in a)May 2008 and b)June 2008.

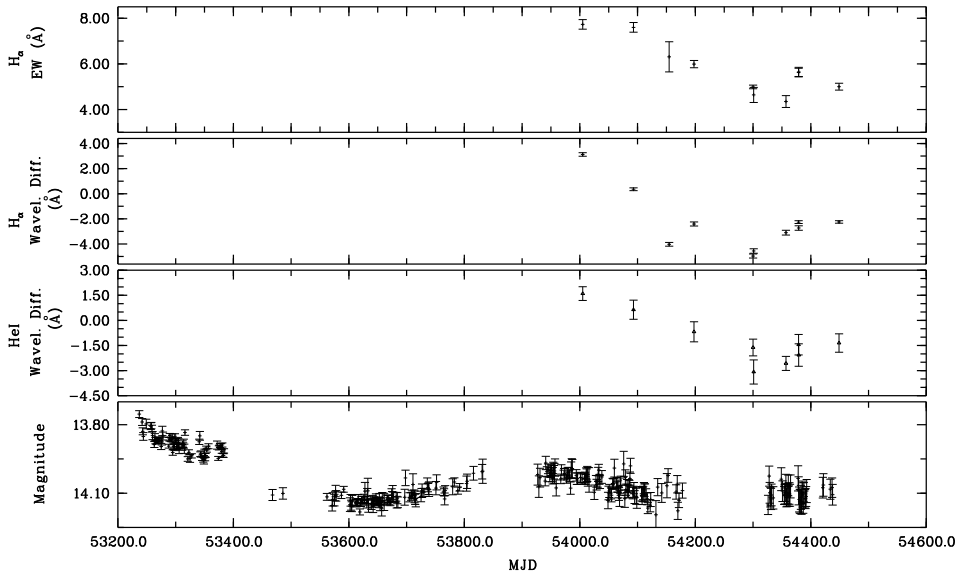

Figure 4.9: The correlation between the EW value of H_α emission line and the optical brightness variation of the source.

peaked, while the EW values continue increasing. The mean EW value of last two observations is 7.04±0.28 Å.

As commonly observed in the spectra of Be stars, the counterpart of GRO J2058+42 also shows variability in V/R (Fig.4.5) and this variations can be explained via global one-armed oscillation model (GOAO) proposed by Okazaki (1991), Papaloizou et al.(1992) and Hanuschik et al. (1995). According to this model V/R variations (it is best seen in the H_α line) occur due to the precession of a perturbation, in the form of a high-density zone, confined in the disk (Okazaki 1997, Telting Kaper 1994). If we assume that the density perturbation revolves in the same direction as the stellar rotation (prograde direction), then the V/R variations should follow such a way which is presented in Fig 4.10. In this figure the direction of the gas and the high-density part of a one-armed oscillation in the disk are represented by curved arrows and grey areas respectively.

Table 4.1: Results of H_α observations for optical counterpart to GRO J2058+42.

MJD	EW (Å)	FWHM (Å)	Vsin(i) (Km/s)	ΔV (Km/s)	Profile Shape
53879.03	1.47±0.32	15.70±4.32	432.22±118.93	435.18	V>R
53945.88	2.71±0.14	8.99±3.82	247.49±105.16	459.86	V<R
53967.04	2.02±0.19	12.84±5.01	353.48±137.92	500.55	V<R
54004.78	2.66±0.18	12.85±5.45	353.76±150.04	402.47	V>R
54266.01	5.43±0.15	14.67±6.23	403.86±171.51	336.90	V<R
54448.81	5.97±0.60	13.99±5.94	385.14±163.53	256.45	V<R
54453.69	5.36±0.39	15.27±5.90	420.38±162.43	369.35	V∼R
54598.95	7.05±0.23	13.56±2.43	373.30±66.90	-	Single
54637.02	7.02±0.32	9.06±3.52	249.42±96.90	-	Single

I) When the high-density zone of the equatorial disk moves towards the observer the emission lines have V>R.

II) If the high-density part of the disk is in front of the star the emission line shows shell profile with maximum central absorption and V=R

III) V<R profile takes place when the high-density region moves away from the observer.

IV) The emission lines have V=R when the profile appears as without a one-armed perturbation. The high-density zone is behind the star in this situation.

The similarity between the shape of the H_α lines in GRO J2058+42 and those predicted by the GOAO model is remarkable except a difference of single-peaked emission profile. The line shapes indicate the following sequence:

$$V>R \rightarrow V<R \rightarrow V<R \rightarrow V>R \rightarrow V<R \rightarrow V<R \rightarrow V=R$$

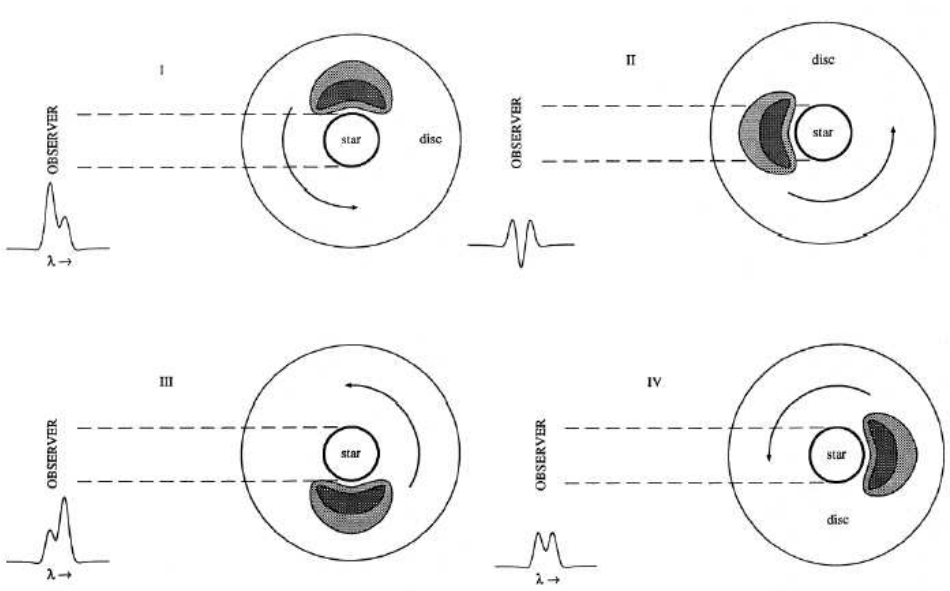

Figure 4.10: Schematic model of V/R variations seen in the spectra of β Mon. Figure taken from Telting et al. (1994).

However the single-peaked emission profile of May 2008 observation has a comprehensible meaning since it was seen at the beginning of the X-ray outburst of the system. It is also interesting that the line profile kept its shape after the outburst. The main difference between the two single-peaked emission lines is that the emission line which is seen after the outburst has a sharp decrease at the red part of its wing and it appears as blue shifted which can be interpreted as the mass loss of a part of high-density zone existing in our line of sight.

Due to the lack of observations which can complete the whole cycle it is quite difficult to state the period of the V/R variation. However, it is clear that according to the evolution of the transitions, period of the V/R variation for the counterpart to GRO J2058+42 should not exceed one year.

4.1.4 Distance and Extinction Estimation

Since we did not observe the counterpart of the system with V filter during the photometric observations we could not determine the amount of the ex-

Table 4.2: Results of the photometric observations of counterpart to GRO J2058+42.

MJD	B	R
53878.98	-	13.96±0.01
53902.81	-	13.96±0.01
53945.81	16.23±0.01	13.96±0.02
53967.00	-	13.97±0.01
53969.00	-	13.96±0.02
54004.76	-	13.98±0.01
54448.79	16.19±0.01	13.70±0.01
54453.65	-	13.70±0.01
54598.93	16.14±0.01	13.66±0.01
54636.90	16.08±0.01	13.62±0.02

tinction of the system using photometric results. For that reason we used the measurements of the EWs of the DIBs to estimate the reddening (Herbig 1975). Choosing the strongest lines at $\lambda\lambda$5778/80, 6202, 6269 and 6613 Å, the mean color excess index was found as *E(B-V)*=1.35±0.18.

$$A_V = R * E(B-V) \tag{4.2}$$

We obtained the extinction of the source A_V=4.46±0.59 using the reddening of R=3.3 for O type stars which is defined in Schmidt-Kaler's (1982) expression . Assuming average absolute magnitude of $M_V = -4.32\pm0.2$ (Vacca et al. 1996), derived for 09.5 V type stars and using the distance-modulus relation,

$$m_v - M_V = 5logd - 5 + A_V \tag{4.3}$$

where m_v is the visual magnitude of the source (m_v=14.9, Reig et al. 2005), d is the distance in units of parsec (pc). The distance to the source is found to be 8.95±1.44 kiloparsecs (kpc). On the other hand the distance is derived as

10.14±1.42 kpc, if the standard reddening value of R=3.1 is used. An estimate of the difference factors mentioned above indicate a range $7.5 \lesssim d \lesssim 11.6$ kpc for the distance to the counterpart of GRO J2058+42. The distance estimate is consistent with the value of Reig et al.(2005) (∼9±1 kpc) and the X-ray distance estimation proposed by Wilson et al. (1998) (7-16 kpc).

The photometric results of the counterpart to GRO J2058+42 are shown in Table 4.2. Photometric results show that the R magnitude of the source has increased during two years with a value of roughly 0.3 magnitude which corresponds to a disk luminosity of about 10^{36} erg s^{-1}. In addition to the enhancement at the R magnitude, the counterpart to GRO J2058+42 has also shown an increase at the B magnitude. The mean value of the measurements was found as B=16.16±0.01 and R=13.85±0.01.

4.2 Results of BQ Cam

4.2.1 Spectral Lines and Comparison with HILTNER 102

Since BQ Cam is much fainter than the counterpart of GRO J2058+42, we used only grism G8 which has a resolution of ∼1.1 Å pix^{-1} for the spectroscopic observations. Therefore several lines that exist in the blue part of the spectrum could not be observed for this source. The long-term light curve of BQ Cam which is obtained using ROTSEIIId archive is presented in Figure 4.11 (provided by Prof. Dr. Ümit Kızıloğlu).

The mid-band spectrum of the source shows that H_α emission line is the most clear line similar to J2058+42's counterpart however with different line profiles (Fig 4.12). HeI λ7065 line which is recognized easily also shows single peak emission in all spectra. The other features which are seen in the spectra are: NaI λ5896 line, strong DIBs at λλ6202 and 6284. They are consistent with the high reddening of the object suggested at the previous works. Neither HeI λ6678 nor HeII lines have been detected in any spectra of BQ Cam.

Comparison of the spectra of the source and the spectrophometric standard

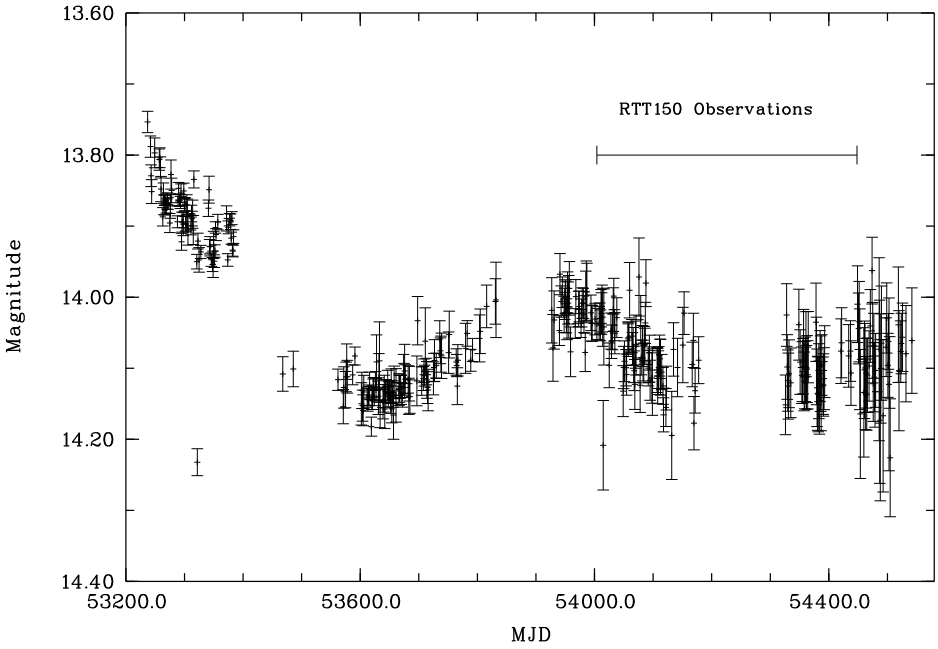

Figure 4.11: Light curve of BQ Cam taken with ROTSEIIId . Duration of RTT150 observations (spectroscopic and photometric) is also remarked with long bar.

star HILTNER 102 is shown in Fig 4.13. As a supergiant star with O9.7 spectral type (Unger 1998) HILTNER 102 has deep HeI $\lambda\lambda$6678 and 7281 absorption lines opposite to BQ Cam. Hα and HeI λ7065 lines are also seen in absorption .

4.2.2 H_α Measurements

H_α emission line which indicates the presence of decretion disk formation in the system appears in all spectra. In addition to H_α emission line, neutral Helium lines at λ7065 Å also show emission feature just in like the other Be stars which exist in the binary systems. The unexpected result is that the evolution of H_α emission lines (Fig.4.14, also Fig.4.15-4.17) throughout the observations which show such a cyclic variation depending on the wavelength. Wrong wavelength calibration which have been done during the reduction of the spectra is thought

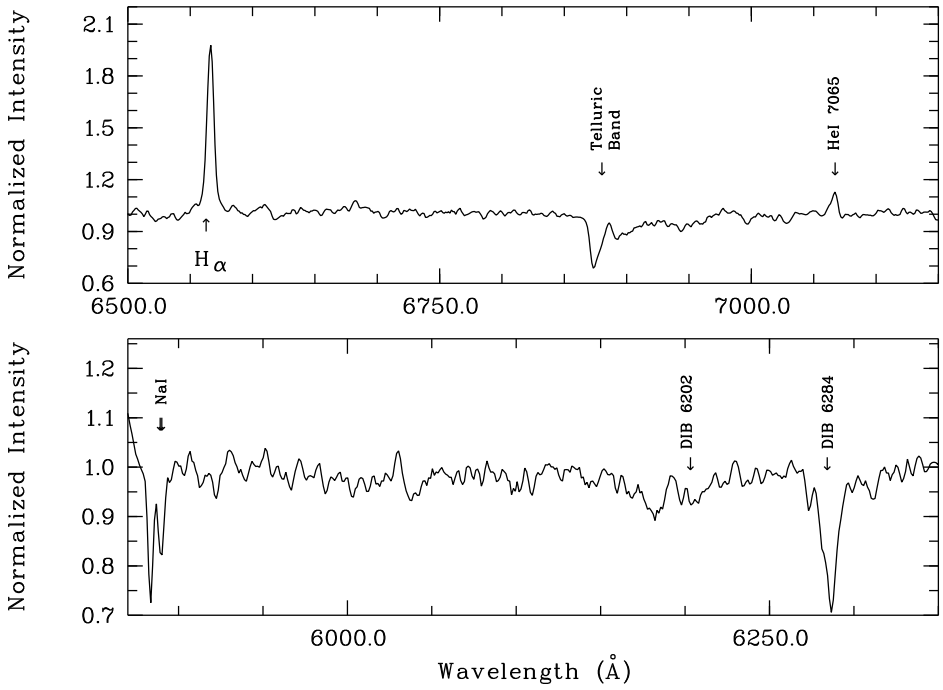

Figure 4.12: Moderate resolution spectra(with G8, resolution ∼3.4) of BQ Cam taken in September 2006.

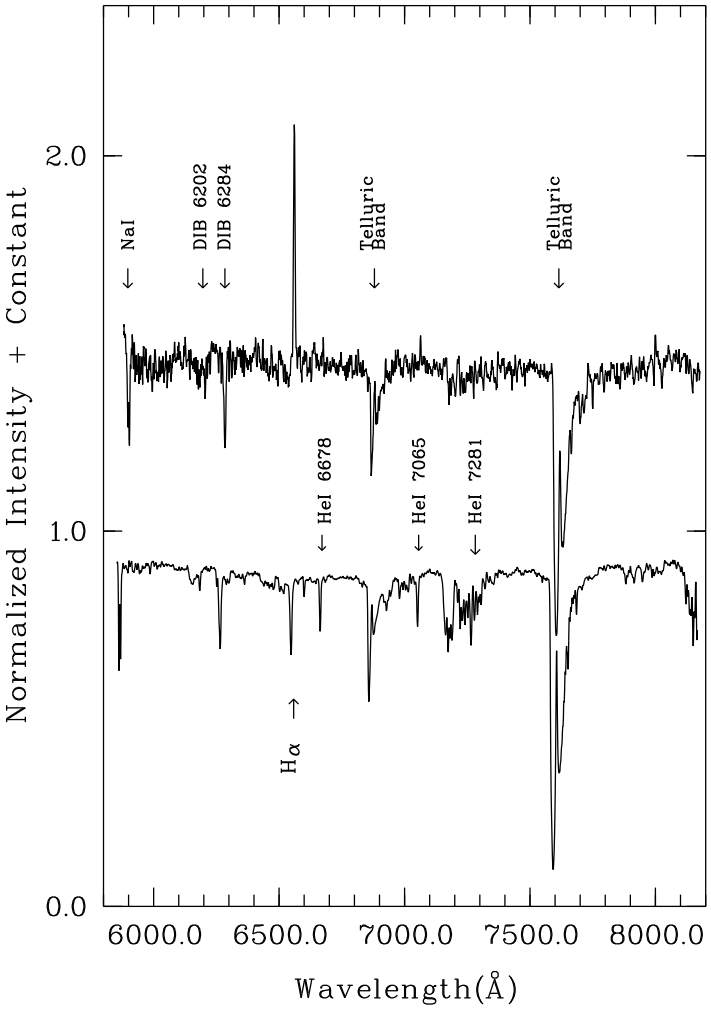

Figure 4.13: The comparison of BQ Cam spectrum (up)taken in December 2007 and HILTNER 102 spectrum (down) taken in June 2007 with G8.

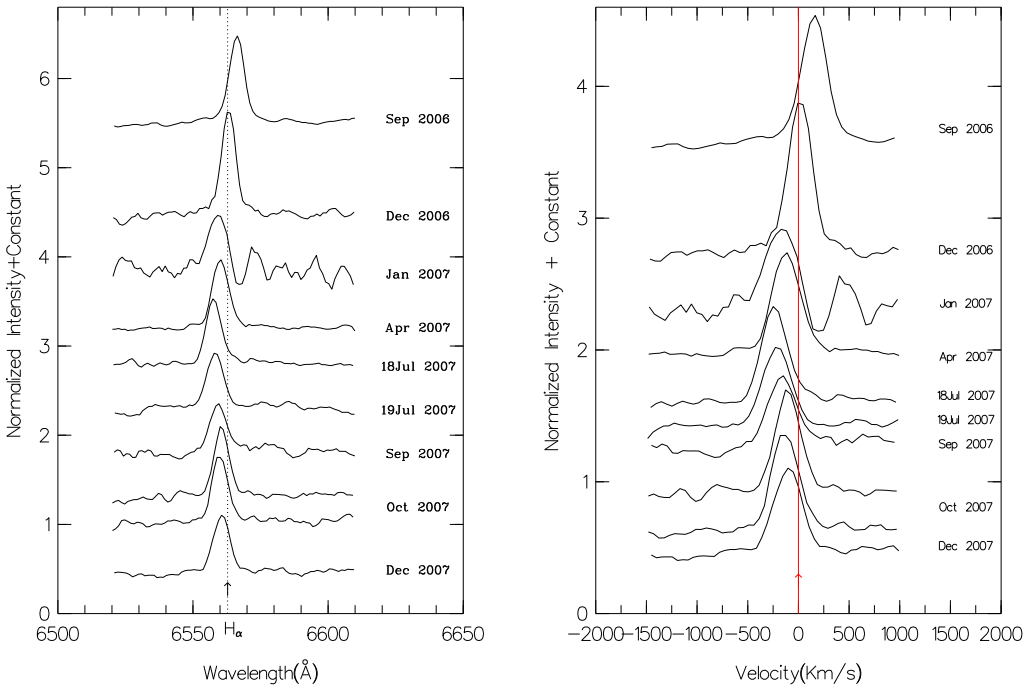

(a) (b)

Figure 4.14: Series of H_α profiles observed between September 2006 and December 2007 (a). The dotted lines represent the laboratory wavelength of H_α line. Note the shifts from the laboratory wavelength show variations changing in the range of (-141) - (+73) km $^{-1}$ (b).

to be the reason of this variation. For this reason the wavelengths of the DIBs which would not be affected from the reduction process have been checked. However it has been found that no line in the spectra shows such an variation except HeI λ7065 line (Fig 4.18).

Furthermore the amount of the variations from the laboratory wavelength of Hα and HeI line are in relation with the EW values of Hα and variation of magnitude of the source during RTT150 observations. Fig 4.19 represnts the EW values of $H_\alpha$line, the amount of wavelength shifts measured for H_α and HeI. The last panel denotes the light curve of BQ Cam which is obtained using ROTSEIIId archive. The general trend seen in the figure is that the EW value

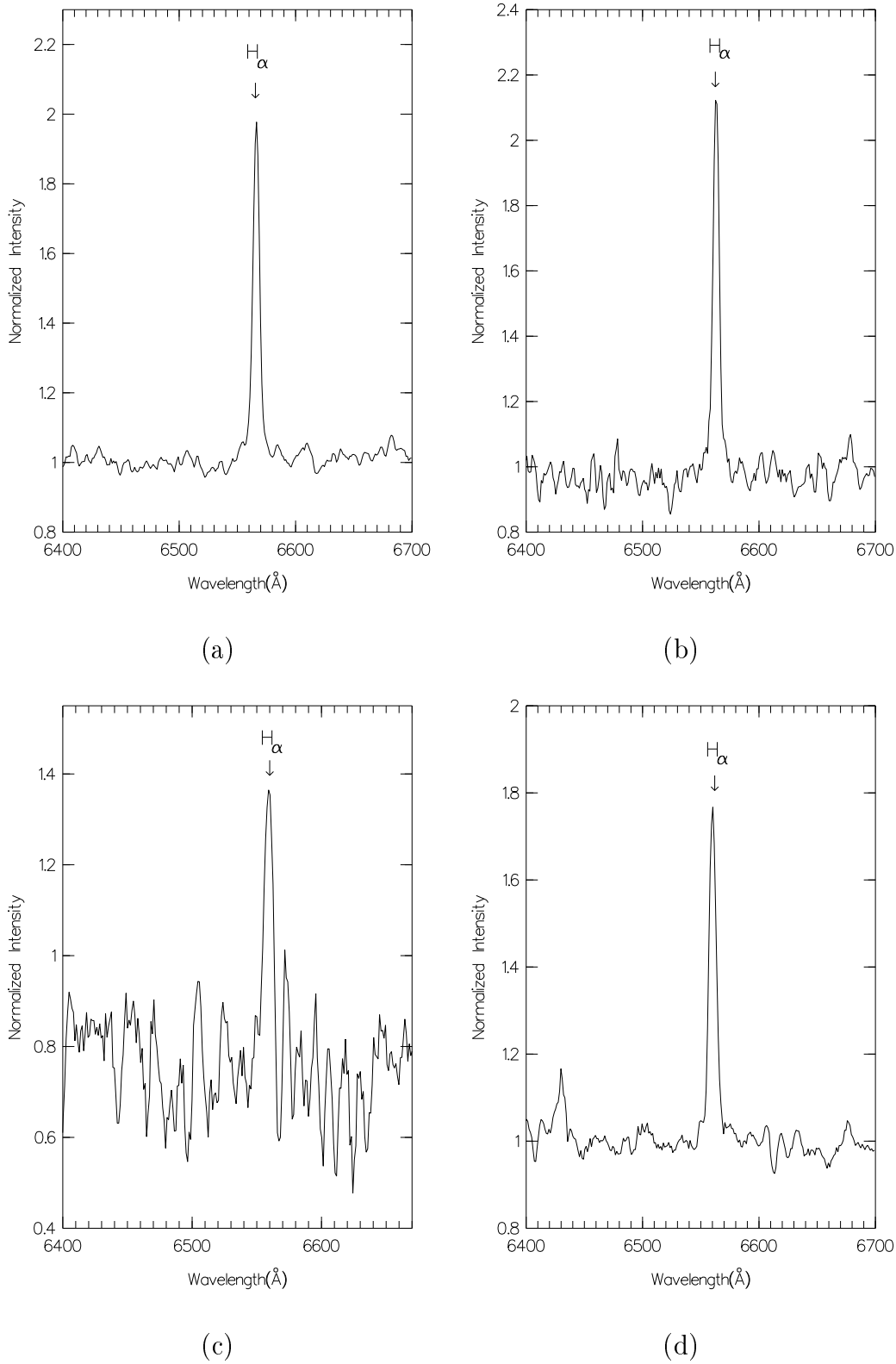

Figure 4.15: H_α profiles of BQ Cam observed in a)September, b)December 2006 and c)January (low SNR), d)April 2007.

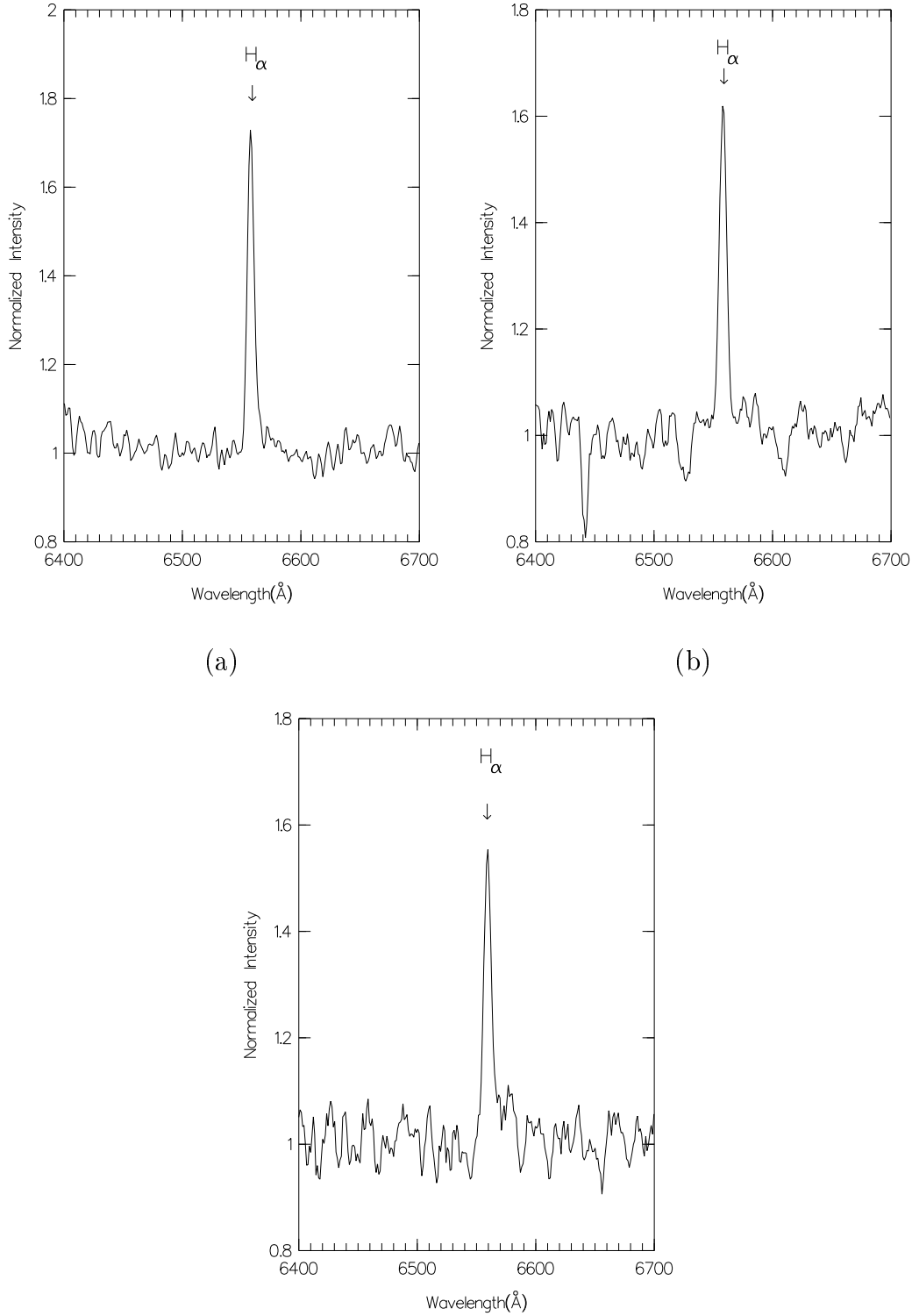

Figure 4.16: H_α profiles of BQ Cam observed on a)18 July, b)19 July 2007 and in c)September 2007.

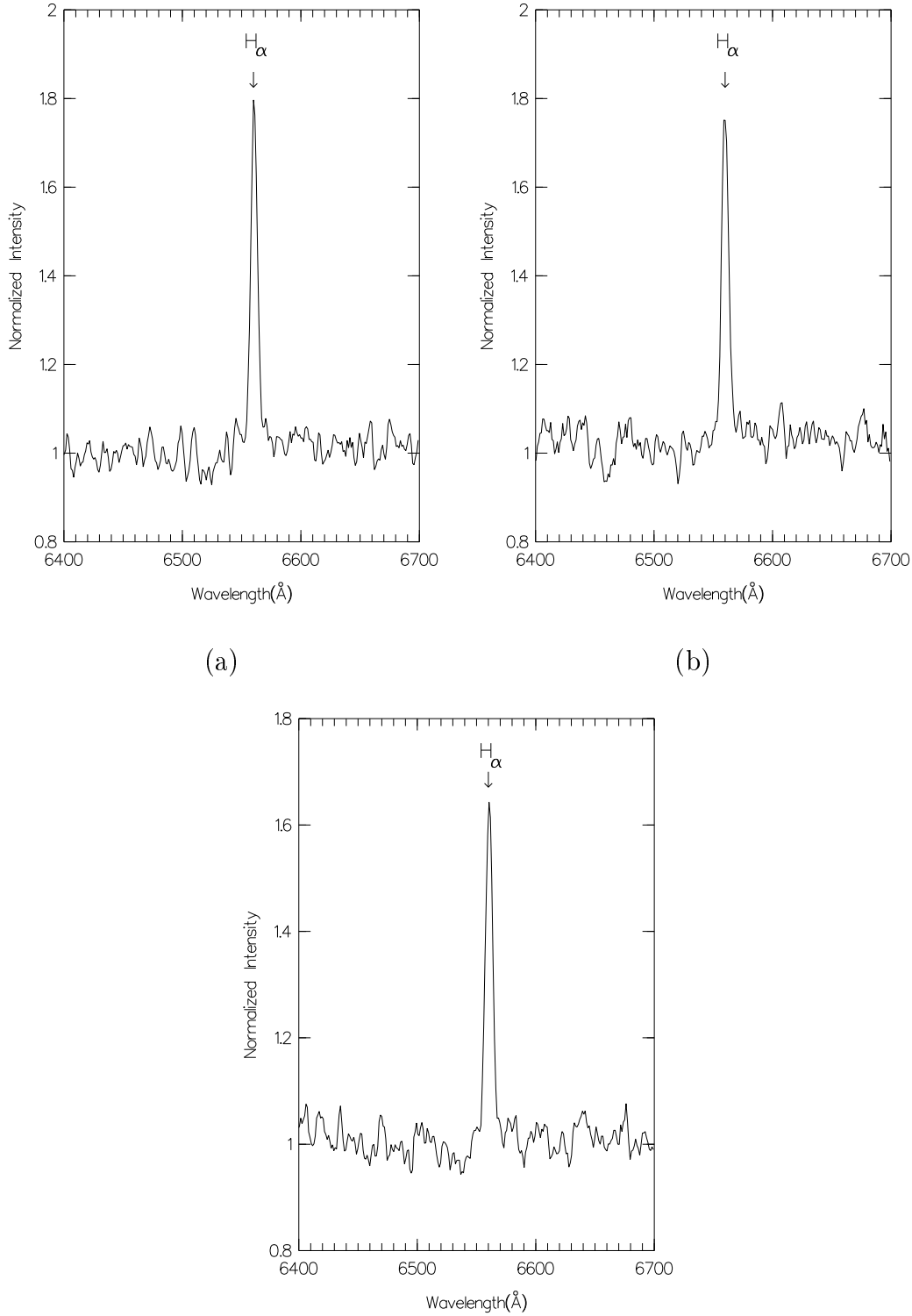

(a) (b)

(c)

Figure 4.17: H_α profiles of BQ Cam observed on 5 October 2007 take part in (a)(b) while (c) represents the December 2007 observation.

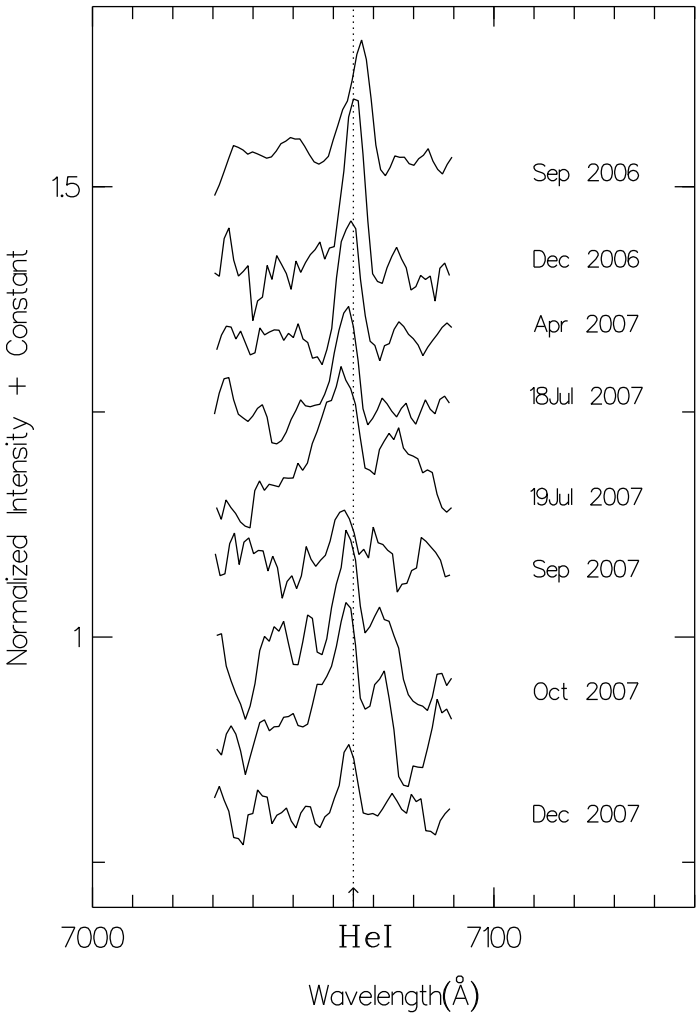

Figure 4.18: Evolution of HeI λ7065 line which was observed between September 2006 and December 2007. The series does not include the January 2007 observation, since the emission line is embedded into the continuum.

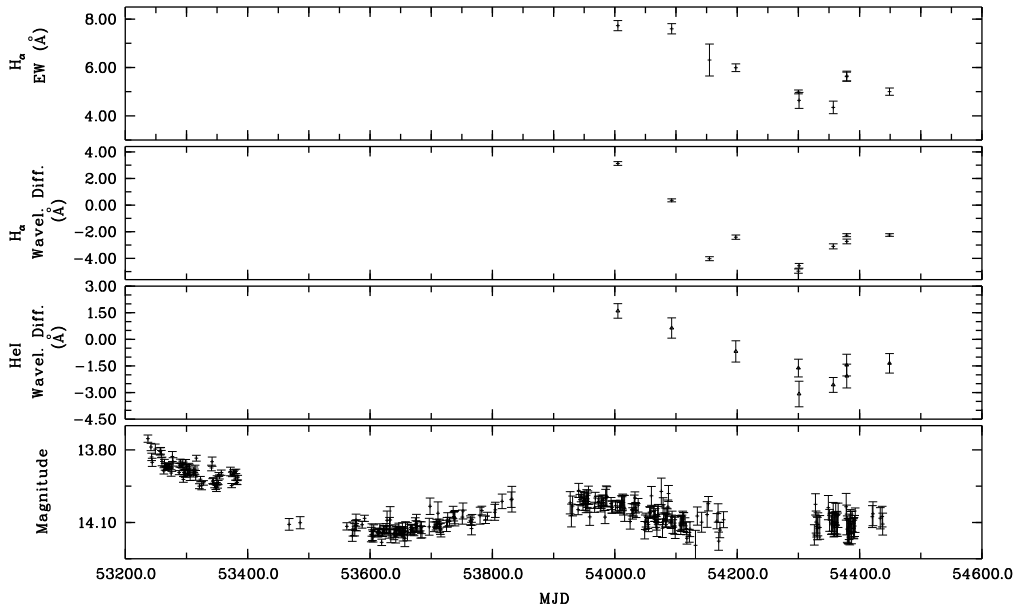

Figure 4.19: The relation between the ROTSEIIId light curve, the EW value of H_α and the the amount of shifts from the laboratory wavelength of the emission lines (H_α and HeI λ7065 lines).

of H_α line decreases as shifts from laboratory wavelengths for the two lines decreases. Since EW value of Hα line is related with the disk density of the Be star rather than its size (Negueruela et al.2001) there might be a decrease in the disk density of BQ Cam. Also it is an obvious evidence for the relation between the EW values of emission lines and the brightness variation of the source mentioned previous work.

Same situation seen in different lines is quite confusing, since the origins of H_α an HeI lines are completely different. The region which is responsible for H_α emission is the outer disk whereas HeI emission line is produced by inner part of the disk. The precession of the whole decretion disk or the orbital plane might be the responsible mechanism for the shift seen at wavelengths for these two lines.

Secondly the existence of a third body in the system may be a probable explanation of the situation though it is a rare phenomenon among the HMXBs. Presence of an apsidal motion for the system V0332+53, defined as rotation of an orbit on its own plane (Petrova and Orlov 1999), was suggested by Zhang et al.(2005). They estimated the angular velocity of the system corresponding to an apsidal period of $\approx 8.6 \times 10^5$ yr as $\dot{W} \sim 5^\circ \times 10^{-3}$ yr^{-1}. Since the angular velocity value of $\sim 1.^\circ 5 \pm 0.8$ yr^{-1} is rather high which is not to be produced by two effects, they also mentioned the probability of the presence of a third body. The results of spectroscopic observations including H_α line are listed in Table 4.3 with its observed wavelength. The mean EW value of H_α derived as 5.79 ± 0.25 Å shows discrepancy with the value of Negueruela et al. (1999) taken in 1997 (EW=3.9 Å). They also suggested the measured V magnitude of the source as 15.73 ± 0.02. However we obtained the mean visual magnitude as 15.43 ± 0.01 (Chapter 4.2.3) from May 2006-December 2007 observations. For that reason, an increase of $\sim$0.3 magnitude in the brightness of the source might be the reason of the discrepancy which is seen in the EW values of H_α emission lines. On the the other hand the EW values have decreased during the observations although the system is still in X-ray quiescent phase since 2004.

Table 4.3: Results of H_α observations of BQ Cam.

MJD	H_α(obs.) (Å)	EW (Å)	FWHM (Å)	Vsin(i) (Km/s)
54004.93	6566.33±0.14	7.73±0.21	7.48±1.00	205.92±27.53
54092.97	6563.18±0.11	7.60±0.21	6.37±0.80	175.36±22.02
54154.70	6558.79±0.15	6.31±0.66	7.00±1.56	192.71±42.95
54197.75	6560.41±0.16	5.99±0.16	7.41±1.32	204.00±36.34
54300.04	6557.86±0.16	4.99±0.08	6.64±1.35	182.80±37.17
54301.07	6558.26±0.18	4.64±0.33	7.21±1.65	198.43±45.42
54357.01	6559.72±0.19	4.35±0.26	7.79±1.96	214.46±53.96
54378.86	6560.56±0.11	5.62±0.19	6.80±1.24	187.20±34.14
54379.07	6560.08±0.18	5.65±0.20	7.08±1.31	194.11±36.06
54448.89	6560.57±0.10	5.00±0.15	7.29±1.55	200.69±42.67

The obtained mean FWHM and Vsin(i) values for H_α line are 7.11±1.37 Å and 195.65±37.83 km s^{-1} whereas 4.91±1.97 and 153.11±54.2 for neutral Helium line. The average of two Vsin(i) values estimated as 174.38±46.02 km s^{-1}. Taking the upper limit of the break-up velocity (V_{break}) for a late O type star as 600 km s^{-1} ($V=0.8V_{break}$), then the orbital inclination angle of V0332+53 would require an value of $i \lesssim 20^\circ$ which is consistent with Zhang et al. (2005).

4.2.3 Distance, Color and Extinction Estimations From Photometric Measurements

We first used the interstellar absorption lines in the spectra, in order to obtain an estimate of the distance d to the system. As the spectroscopic results of BQ Cam does not cover the blue range of the spectrum we had just two strong DIBs presented at $\lambda\lambda$6202 and 6284 Å. Applying the approximation of Herbig (1975) to the derived EW values of the DIBs, we have found the color excess of

Table 4.4: Photometric measurements of BQ Cam.

MJD	B	R	V
54004.92	-	14.18±0.01	-
54092.95	-	14.26±0.01	-
54123.68	17.13±0.01	14.27±0.01	15.44±0.01
54197.73	17.15±0.01	14.25±0.02	15.44±0.01
54300.02	17.16±0.01	14.35±0.01	15.44±0.01
54301.05	-	14.36±0.01	-
54356.99	17.11±0.01	14.33±0.01	15.42±0.01
54378.93	17.15±0.01	14.69±0.02	15.46±0.02
54448.87	17.13±0.01	14.28±0.01	15.39±0.01

the source as *E(B-V)*=1.85±0.16 which is above the value of J2058+42.

Using the standard reddening of R=3.1 and the absolute magnitude M_V=-4.66 (Vacca et al. 1996) estimated for O8V type stars, we derive a distance $d\approx$9 kpc whereas Schmidt-Kaler's expression for the reddening to late O type stars R=3.3 gives a distance of $d\approx$6 kpc.

We derived the mean observed color index as (B-V)=1.71±0.02. Using the intrinsic color index for O8V type star is $(B\text{-}V)_0$=-0.285 (Wegner 1994), the color excess gives the result of *E(B-V)*=2.00±0.02 on the other hand. The comparatively higher reddening obtained from the photometric magnitudes may be explained by the contribution of the decretion disk of Be star, as the DIBs should be free of such effects (Wilson et al. 2005).

Taking the standard law for extinction (reddenning R=3.1) the distance to the source estimated to be ≈6 kpc while R=3.3 gives the distance $d\approx$5 kpc. Although the derived distance estimations are slightly different, these values are almost close to the range of $6\lesssim d\lesssim 9$ kpc proposed by Negueruela et al. (1999).

Additionally, the mean value of B,and R magnitudes have been found as B=17.14±0.01 and R=14.33±0.01. Although derived mean R magnitude is

almost identical with the USNO B1.0 catalogue, the Be star shows a decrease of 0.1 magnitude during Sept 2006-December 2007 which is also consistent with the ROTSEIIId light curve.

CHAPTER 5

CONCLUSIONS

We have presented the optical spectroscopic and photometric observations of the counterpart to the systems GRO J2058+42 and V0332+52 (BQ Cam) in this work.Detection of the H_α emission line feature seen in the spectrum points out the presence of the decretion disk existence for the counterparts of both sources. The distance and extinction estimations obtained with the spectroscopic observations are also consistent with the previous works. The distance to the counterpart of GRO J2058+42 was found in the range of $7.5 \lesssim d \lesssim 11.6$ kpc using the EW values of DIBs. However it was determined as $6 \lesssim d \lesssim 9$ kpc for BQ Cam.

As an O9.5-B0 IV-V type star,counterpart to GRO J2058+42 has an double-peaked H_α profiles during May 2006-December 2007 observations whereas following two spectra have single-peaked emissions which have never been detected before. It is also noteworthy that the results of the spectroscopic and photometric observations achieved during the onset of the last X-ray activity (Krimm et al. 2008) of the system have been declared for the first time. The Be star of the system indicates an V/R variation which can be explained by the prograde global one-armed oscillation model. Before the outburst, the EW value of the emission line and R magnitudes reaches a maximum which can be thought as the indicators of the following May 2008 X-ray activity. Since the last X-ray outburst was a normal outburst we have assumed that a loss of a large amount of the material would not become at the decretion disk of the Be star. So the

EW value of H_α line which remains nearly same after the outburst is compatible with this assumption. A close correlation between the EW values of H_α emission lines and the brightness variations for the optical counterpart to GRO J2058+42 was also seen at the spectroscopic results.

The spectroscopic results of BQ Cam, a main sequence star with the spectral type O8-O9, point out that the H_α and HeI λ7065 lines have single-peaked emissions. The most remarkable outcome of this work may be the determination of the existence of the wavelength shifts seen at H_α and HeI emission lines, produced by the different parts of the disk, with an almost cyclic appearance. However additional observations are needed to determine the period of these variations. In addition, the equivalent width values of H_α emission lines, shifts from the the laboratory wavelengths for H_α and HeI emission lines and the variation in the optical brightness of BQ Cam show a close correlation. The correlation between the EW values of H_α emission lines and the brightness variations for the optical companion is also seen in the case of the optical counterpart to GRO J2058+42. However it is unexpected to see the similar correlation for the shifts from the laboratory wavelengths of H_α and HeI emission lines. Therefore it is quite difficult to specify the mechanism that gives rise to these shifts and the defined correlation. One possible explanation is the precession of the disk which includes a high density zone or tunnel. The high density zone, which is the responsible mechanism of V/R variations in GOAO model, may lie from the inner to outer part of the disk unlike other Be stars, so we see the same variations at H_α and HeI lines. The second scenario is the existence of an third body in the system. The presence of an apsidal motion, generally related with triple systems, have been announced in V0332+53 might be an evidence of this fact. However X-ray and long-term optical photometric observations of the system are needed to prove this idea.

REFERENCES

[1] Baade D., 1982, A&A, 105, 65

[2] Baade D., Rivinius Th., Štefl S., 2002b, A&A, 383, 31

[3] Bernacca P. L., 1983, IAU Circ., 3904

[4] Bernacca P. L., Iijima T., Stagni R., 1984, A&A, 132, L8

[5] Bjorkman J. E., Cassinelli J. P., 1993, ApJ, 409, 429

[6] Buscombe W., 1969, MNRAS, 144, 1

[7] Campana S., Stella L., Moretti A., Parmar A. N., Orlandini M., 2002, ApJ, 580, 389

[8] Cassinelli J. P., Brown J. C., Maheswaran M., Miller N. A., Telfer D. C., 2002, ApJ, 578, 951

[9] Charbonneau P., MacGregor K. B., 2001, ApJ, 559, 1094

[10] Collins G. W., 1987, IAU Colloquium 92, Physics of Be Stars, ed. Slettebak A. and Snow T. P., Cambridge University Press, 3

[11] Corbet R. H. D., 1984, A&A, 141, 91

[12] Corbet R. H. D., 1986, MNRAS, 220, 1047

[13] Corbet R. H. D., Charles P. A., van der Klis M., 1986, A&A, 162, 117

[14] Corbet R., Peele A., Remilliard R., 1997, IAU Circ., 6556

[15] Finger M. H., Wilson R. B., Harmon B. A., 1996, ApJ, 459, 288

[16] Finger M. H., Prince T. A., 1997, Proceedings of the Fourth Compton Symposium, AIP, Woodbury, NY, part 1, 57

[17] Goraya P. S., Rautela B. S., 1985, Ap&SS, 113, 373

[18] Hanuschik R. W., Hummel W., Dietle O., Sutorius E., 1995, A&A, 300, 163

[19] Hanuschik R. W., 1996, A&A, 308, 170

[20] Heger A., Langer N., 2000, ApJ, 554, 1016

[21] Herbig G. H., 1975, ApJ, 196, 120

[22] Honeycutt R. K., Schlegel E. M., 1985, PASP, 97, 300

[23] Huang S. S., 1972, ApJ, 171, 549

[24] Jaschek M., Egret D., 1982, Proceedings of IAU Symposium 98, 261

[25] Kızıloğlu Ü., Kızıloğlu N., Baykal A., Yerli S. K., Özbey M., 2007, A&A, 470, 1023

[26] Kızıloğlu Ü., Kızıloğlu N., Baykal A., Yerli S. K., Özbey M., 2008a, IBVS, 5821

[27] Kızıloğlu Ü., Kızıloğlu N., Baykal A., Yerli S. K., Özbey M., 2008b, ATel, 1717

[28] Kreykenbohm I., Mowlavi N., Produit N., Soldi S., Walter R., et al. 2005, A&A, 433, L45

[29] Krimm H. A., Barthelmy S. D., Baumgartner W., Cummings J., Fenimore E., et al. 2008, ATel, 1516

[30] Lee U., Saio H., Osaki Y., 1991, MNRAS, 250, 342

[31] Maeder A., 1999, A&A, 347, 185

[32] Makishima K., Ohashi T., Kawai N., Matsuoka M., Koyama K., et al. 1990, PASJ, 42, 295

[33] Motch C., Stella L., Janot-Pacheco E., Mouchet M., 1991, ApJ, 369, 490

[34] Negueruela I., Reig P., Coe M. J., Fabregat J., 1998, A&A, 336, 251

[35] Negueruela I., Roche P., Fabregat J., Coe M. J., 1999, MNRAS, 307, 695

[36] Negueruela I., Okazaki A. T., 2000, ASPC, 213, 714

[37] Negueruela I., Okazaki A. T., Fabregat J., Coe M. J., Munari U., Tomov T., 2001, A&A, 470, 1023

[38] Negueruela I., 2004, arXiv:astro-ph/0411335

[39] Okazaki A. T., 1991, PASJ,43, 75

[40] Okazaki A. T., 1997, A&A, 318, 5480

[41] Okazaki A. T., 2001, PASJ, 53, 119

[42] Okazaki A. T., Negueruela I., 2001, MNRAS, 377, 1610

[43] Okazaki A. T., Negueruela I., 2001, ASPC, 234, 281

[44] Owocki S. P., Cranmer S. R., Blondin J. M., 1994, ApJ, 424, 887

[45] Owocki S. P., Cranmer S. R., Gayley K. G., 1996, ApJ, 472, L115

[46] Owocki S. P., ud Doula A., 2003, ASPC, 305, 350

[47] Papaloizou J. C., Savonije G. J., Henrichs H. F., 1992, A&A, 265, L45

[48] Petrova A. V., Orlov V. V., 1999, AJ, 117, 587

[49] Popov S. B., Raguzova N. V., 2004, arXiv:astro-ph/0405633

[50] Porter J. M., 1998, A&A, 336, 966

[51] Porter J. M., 1999, A&A, 348, 512

[52] Porter J. M., Rivinius T., 2003, PASP, 115, 1153

[53] Raguzova N. V., Lipunov V. M., 1998, A&A, 340, 85

[54] Reig P., Fabregat J., Coe M. J., 1997, A&A, 322, 193

[55] Reig P., Kougentakis T., Papamastorakis G., 2004, ATel, 308

[56] Reig P., Negueruela I., Papamastorakis G., Manousakis A., Kougentakis T., AA, 440, 637R

[57] Reig P., Martínez-Núñez S., Reglero V., 2006, A&A, 449, 703

[58] Remillard R., 2004, ATel, 371

[59] Rivinius Th., Baade D., Štefl S., 2003, A&A, 411, 229

[60] Scargle J. D., Erickson E. F., Witteborn F. C., Strecker D. W., 1978, ApJ, 224, 527

[61] Schmidt-Kaler Th., 1982, BICDS, 23, 2S

[62] Slettebak A., 1978, SSR, 23, 541

[63] Slettebak A., 1988, PASP, 100, 770

[64] Stella L., White N. E., 1983, IAU Circ., 3902

[65] Stella L., White N. E., Davelaar J., Parmar A. N., van der Klis M., Blissett R. J., 1985, ApJ, 288, L45

[66] Stella L., White N. E., Rosner R., 1986, ApJ, 308, 669

[67] Stocke J., Silva D., Black J. H., Kodaira K., 1985, PASP, 97, 126

[68] Struve O., 1930, ApJ, 72, 1

[69] Struve O., 1931, ApJ, 73, 94

[70] Takeshima T., Dotani T., Mitsuda K., Nagase F., 1994, ApJ, 436, 871

[71] Tanaka Y., 1983, IAU Circ., 3891

[72] Telting J. H., Heemskerk M. H. M., Henrichs H. F., Savonije G. J., 1994, A&A, 288, 558

Telting J. H. and Kaper L., 1994, AA, 284, 515,

[73] Terrell J., Priedhorsky W. C., Davelaar J., Blissett R., Stella L., et al. 1983, IAU Circ., 3893

[74] Terrell J., Priedhorsky W. C., 1984, ApJ, 285, 15

[75] Vacca W. D., Garmany C. D., Shull J. M., 1996, ApJ, 460, 914

[76] van den Heuvel E. P. J., Rappaport S., 1987, IAU Colloquium 92, Physics of Be Stars, eds. Slettebak A. and Snow T. P., Cambridge University Press, 21

[77] Vogt S. V., Penrod G. D., 1983, ApJ, 275, 661

[78] Unger S. J., Roche P., Negueruela I., Ringwald F. A., Lloyd C., Coe M. J., 1998, A&A, 336, 960U

[79] Whitlock L., 1989, ApJ, 344, 371

[80] Wegner W., 1994, MNRAS, 270, 229

[81] Williams P. M., Brand P. W. J. L., Bell-Burnell S. J., Webster A. S., 1983, IAU Circ., 3904

[82] Wilson C. A., Zhang S. N., Finger M. H., Wilson R. B., Scott M., et al. 1995, IAU Circ., 6238

[83] Wilson C. A., Strohmayer T., Chakrabarty D., 1996, IAU Circ., 6514

[84] Wilson C. A., Finger M. H., Harmon B. A., Chakrabarty D., Strohmayer T., 1998, ApJ, 499, 820

[85] Zhang S., Qu J. L., Song L. M., Torres D. F., 2005, ApJ, 630, L65

[86] Ziólkowski J., 2002, MmSAI, 73, 1038